

THE DETERMINATION OF THE CRYSTAL  
STRUCTURE OF POTASSIUM PICRATE

Thesis by  
Max Bettman

In Partial Fulfillment of the Requirements  
for the Degree of  
Doctor of Philosophy

California Institute of Technology  
Pasadena, California

1952

## ACKNOWLEDGEMENT

I wish to express my sincere appreciation for the help and guidance received from Dr. Edward W. Hughes and Dr. Jerry Donohue. Dr. Hughes suggested the problem and supervised it until his departure for England on a year's leave of absence. Dr. Donohue then took over the supervision.

This work was supported in its later and most costly stages by a grant from the Naval Ordnance Test Station at China Lake, California. Special thanks are due to Drs. Burkhardt and Bryden of this station for taking two photographs which could not be obtained at the California Institute of Technology because of instrumental limitations.

## ABSTRACT

The crystal structure of potassium picrate has been determined and refined to a considerable degree of accuracy by means of x-ray diffraction techniques. Most of the refinement was carried out by the use of least squares methods, by making use of about half of the three dimensional data obtainable from copper  $K\alpha$  radiation.

The benzene ring of the picrate ion is nearly planar, the deviation from planarity being within experimental error. The para nitro group is twisted  $6^\circ$  out of the plane of the benzene ring, apparently due to ionic attraction of the oxygen atoms to neighboring potassium ions. The ortho nitro groups are twisted  $27^\circ$  out of the plane of the benzene ring due to steric hindrance between the phenol oxygen and its two nearest oxygen neighbors in the ortho nitro groups. Chemical bonds of a given species, such as carbon-carbon bonds, show considerable variations in length. All these variations are quite reasonable in the light of well known principles of structural chemistry.

The packing of the structure seems to be largely determined by the ionic attraction between potassium ions and five out of the seven oxygen atoms of each picrate ion. There also exist some rather short van der Waals contacts between neighboring picrate ions.

## TABLE OF CONTENTS

<u>PART</u>	<u>TITLE</u>	<u>PAGE</u>
I	THE DETERMINATION OF THE CRYSTAL STRUCTURE OF POTASSIUM PICRATE . . . . .	1
	INTRODUCTION . . . . .	1
	EXPERIMENTAL . . . . .	4
	Crystal Growth . . . . .	4
	Crystal Habit . . . . .	4
	Density . . . . .	5
	Crystal Mounting and X-ray Photography	6
	Intensity Data . . . . .	9
	Experimental Work on Ammonium Picrate.	11
	UNIT CELL AND SPACE GROUP DETERMINATION . .	12
	The Approximate Unit Cell Dimensions .	12
	Accurate Unit Cell Dimensions . . . .	12
	Determination of the Space Group . . .	15
	Space Group Requirements . . . . .	15
	Number of Molecules per Unit Cell . .	16
	DETERMINATION OF THE TRIAL STRUCTURE . . .	17
	THE REFINEMENT OF THE STRUCTURE . . . . .	28
	Determination of Scale and Temperature Factors . . . . .	28
	The Half-cell Fourier Projection onto (001). . . . .	32
	Refinement of the Structure by Least Squares Methods . . . . .	40
	Methods of Calculation . . . . .	42
	Weighting of the Observational Equations . . . . .	43
	Resulting Parameters . . . . .	46
	DESCRIPTION AND DISCUSSION OF THE STRUCTURE	64
	Internal Configuration of the Picrate Ion . . . . .	64
	The Packing of Potassium Picrate . . .	70
	Comparison with Similar Structures . .	85
	REFERENCES . . . . .	89
	PROPOSITIONS . . . . .	90

THE DETERMINATION OF THE CRYSTAL STRUCTURE  
OF POTASSIUM PICRATE

INTRODUCTION

Multi-nitrated benzenes have interesting properties, such as their ability to form addition complexes with many types of aromatic substances. Such addition complexes cannot be explained on the basis of chemical binding and may therefore be entirely due to the physical properties of the nitrated benzenes. It is important, therefore, to collect accurate structural data from which many of the characteristics of these molecules, such as the nature of their various chemical bonds and the probable charge distribution might then be inferred.

Several structure determinations of compounds of this type have been carried out. Paradinitrobenzene has been studied by James, King, and Horrocks<sup>(1)</sup>, by Llewellyn<sup>(2)</sup>, and by Abrahams<sup>(3)</sup>. Powell<sup>(4)</sup> has determined the structure of picryl iodide. Grison<sup>(5)</sup> reported structures for three polymorphic forms of N-picryl paraiodoaniline. The crystal structure of metadinitrobenzene has been worked out by Archer<sup>(6)</sup> as well as by Gregory and Lasette<sup>(7)</sup>. The structure of paranitroaniline has been determined by Abrahams and Robertson<sup>(8)</sup>.

In all these cases, however, the accuracy obtained was not up to the best modern standards, and the values of the individual bond lengths and bond angles which were determined are believed to be rather unreliable, even though the gross aspects of these structures have been solved. All but two of them were done by two dimensional Fourier projections and all of them were done without corrections for the termination of the Fourier series. Grison used some three dimensional sections in addition to his two dimensional projections, but he estimates his own accuracy as only about  $\pm 0.05 \text{ \AA}$  for interatomic distances. This uncertainty is presumably due to the presence of the strongly scattering iodine atoms. Llewellyn used three dimensional Fourier series and his work should have been reasonably accurate. For some reason which is not quite clear, however, there seems to be some doubt concerning the accuracy of his results (see discussion in subsequent paper on p-dinitrobenzene by Abrahams<sup>(3)</sup>). His average discrepancy between calculated and observed structure factors is 24% which is rather high. His calculations contain some errors, so that the reported geometry of his molecule is not compatible with his own parameters.

For the present work, potassium and ammonium picrate were originally chosen to be determined simultaneously by the isomorphous replacement technique. The optical data and axial ratios listed in Groth<sup>(9)</sup> indicated that the two salts might be isomorphous. Preliminary x-ray work showed

that they have the same space group and closely similar unit cell dimensions. During further work, however, there developed some doubt as to the exact similarity of the two structures. Moreover, it became clear that the isomorphous replacement technique was not well suited for this problem, even if the two structures were strictly isomorphous. At the same time it was learned that another group of investigators\* were working on ammonium picrate. For this reason, our work was switched entirely to the potassium salt.

There is an additional point of interest in ammonium and potassium picrate. When these salts are prepared by the neutralization of picric acid with the corresponding base, the color of the crystals ranges from light yellow to a deep orange. The darker colors seem to be due to an impurity which is produced by overheating the salt solution in an excess of base. During the preliminary work carried out by Dr. E. W. Hughes at this Institute, it was found that the orange crystals give the same diffraction patterns as the yellow ones and are therefore not a polymorphic variety of the latter, but rather a solid solution of the impurity in the picrate. It seems reasonable to suppose that the impurity is structurally similar to the picrates, and that the structure determination of potassium picrate may be the first step toward an eventual isolation and identification of the impurity.

---

\* Donnay and Benkelman at Johns Hopkins University.

## EXPERIMENTAL

### Crystal Growth\*

Equimolar quantities of commercial picric acid and potassium hydroxide were weighed. The picric acid was dissolved in water at elevated temperatures and the hydroxide was then added. The volume of the solution was adjusted until the solution was saturated at 50°-60° C. The crystals of potassium picrate were grown by slowly cooling this solution.

Heating at higher temperatures with an excess of hydroxide produces a red solution and red crystals. Actually, the color can be darkened to a dark brown if a sufficiently large excess of base and sufficiently high temperatures are used. Dr. Hughes purposely prepared some red crystals and verified the fact that they give diffraction patterns identical to those obtained from the yellow crystals. It was assumed, therefore, that the overheating in excess base produces an impurity which forms dilute solid solutions with the picrate, causing a darkening of the color, but otherwise not affecting the properties of the crystal materially, as long as it is present in small amounts. Subsequently, all diffraction experiments were carried out with golden yellow and presumably pure potassium picrate crystals.

### Crystal Habit

All crystals grown in this manner were long needles,

\* The crystals were grown by Dr. E. W. Hughes prior to this writer's work on the problem.

with their needle axes parallel to  $c_0$ . The average dimensions of the crystals were of the order of 1-2 mm along the needle axis and 0.1 mm in mean diameter. The most prominent faces are the set  $\{110\}$ .  $\{100\}$  and  $\{010\}$  also were observed in some of the crystals, though with less prominence. No other faces were observed in the  $\{001\}$  zone. Faces in other zones were not observed, since they can occur only at the two ends of the long thin needles and therefore have very small areas. However, the habits of well developed crystals of potassium and ammonium picrates, carefully grown from different solvents, are described in Groth<sup>(9)</sup>. The cross sections of most of our crystals were approximately diamond shaped, with diagonals of unequal length. Insofar as possible, crystals were picked out with nearly equal diagonals so that the crystals were as close to being cylindrical as possible, in order to minimize absorption errors.

### Density

The density of potassium picrate was determined by the flotation method. Mixtures of propylene bromide, ethylene bromide, and methylene iodide were used. A mixture of two components is enough, of course, as long as one has a higher and the other a lower density than the crystals. Several crystals were dumped into these liquids and the mixture was adjusted until the densest crystals just floated. The density of the liquid was then determined pycnometrically. The flotation was carried out in a large water bath at room

temperature in order to decrease temperature fluctuations. The density determined in this way was found to be 1.940 g/cc.

### Crystal mounting and x-ray photography

All photographs involving rotation or oscillation of crystals around their  $c_0$  axes were made with uncut and unground crystals. The crystals were picked out with some care to obtain reasonably constant diameters, as mentioned before. They were mounted on glass fibers with their needle axes parallel to the fiber. Flake shellac, melted with a hot wire, was used as a cement. Both ammonium and potassium picrates are quite stable at the temperatures necessary to melt the shellac.

The mounted crystals were generally lined up on an optical goniometer. The lining up was then sometimes tested by taking Laue photographs and centering the symmetry elements. Two  $24^\circ$  oscillation pictures around  $c_0$  were taken on a camera of 5 cm. radius. These were made for the purpose of measuring the unit cell axes  $a_0$  and  $b_0$  accurately. Actually, each photograph was a superposition of two equally exposed  $24^\circ$  oscillation ranges, related to each other so as to produce the same reflections on the left as on the right side of the picture in order to remove the ambiguity concerning the position of the center of the photograph.

For the measurement of intensities, only equi-inclination Weissenberg photographs were used. A good description of the camera setup in this type of photography is given, for

instance, by Buerger<sup>(10)</sup>. Equi-inclination photographs of the zero or equatorial, the first, and the 3rd layer around the  $c_0$  axis were taken. The 5th layer required an inclination angle in excess of the maximum inclination for which the cameras at this Institute can be set. It was kindly taken for us at the Naval Ordnance Test Station at China Lake. For all Weissenberg photographs two or three films were inserted into the camera in accordance with the multiple film technique of DeLang, Robertson and Woodward<sup>(11)</sup>, which facilitates the measurements of intensities.

Two more multiple film equi-inclination Weissenberg photographs were taken around the  $b_0$  axis, namely the equatorial and the second layer. For the purpose of taking intensity pictures around the  $b_0$  axis, a crystal had to be cut and ground in order to reduce absorption errors. A thick needle was selected and cut, by means of a razor blade, to a length roughly equal to the maximum diameter. The crystal fragment was then mounted on one of its edges such that the  $b_0$  axis was vertical. The crystal was then ground mechanically on an abrasive wheel, in a crystal grinder designed for this purpose. The ground crystal consisted of a cylindrical central section plus wedge shaped ends, the remnants of the  $\{110\}$  faces.

In addition, one single-film ( $h0l$ ), i.e. equatorial, Weissenberg photograph was taken around  $b_0$  for the purpose of exact measurement of the lengths of the  $c_0$  and  $a_0$  axes.

Some shop-built adaptors were used to insure the tight pressing of the film against the back of the camera. The camera radius had previously been determined by Dr. Pasternak, who found it to be satisfactorily constant along the length of the camera. In this manner accurate measurements of cell edges can be made from conveniently indexed Weissenberg photographs which are normally considered too inaccurate for this purpose.

The Weissenberg cameras used were of the "undistorted scale" described in Buerger, with a 57.3 mm diameter and a camera translation of 0.5 mm per degree of rotation of the crystal. Copper radiation was used for all rotating crystal photographs. In some cases nickel filters were used to decrease the intensity of the  $\text{Cu K}\beta$  line relative to that of the  $\text{K}\alpha$  lines. It was always possible to differentiate between  $\alpha$  and  $\beta$  reflections. However, in the unfiltered Weissenberg photographs there were usually a few partial or complete coincidences of  $\alpha$  and  $\beta$  spots of different indices, a situation which made the intensity measurement of these spots difficult. On the other hand, the presence of  $\text{K}\beta$  spots made it possible to measure some high angle reflections whose corresponding  $\text{K}\alpha$  reflections are ruled out. A reasonable exposure time is of the order of three hours under the following conditions: (i)  $180^\circ$  oscillation, (ii) unfiltered radiation, (iii) 57 mm diameter camera, (iv) a crystal of the dimensions previously described, rotated about the  $c_0$  axis for an equatorial layer photograph, (v) use of a hot filament copper tube run at a 35 KV peak and a space current of 20 m.a.

## Intensity Data

Intensity measurements were made exclusively from Weissenberg photographs by visual estimation. For this purpose a combination of the multiple film method of De Lang, Robertson, and Woodward<sup>(11)</sup> with the intensity strip method was used. The multiple film method usually consisted of placing three films in the camera and resulted in a great expansion of the range of measurable intensities. Intensities can be measured only within a limited region of blackness of the reflections. A minimum blackening is required to distinguish them from the diffuse background. Above a certain practical maximum, the amount of light transmission does not further decrease measurably with increasing degree of exposure. By using three films in a series, the first film can be used for measuring the weakest spots. The strongest spots, which are too black on the first film, are measured on the third film. Each layer of the Kodak No-Screen x-ray film used in this laboratory reduces normally impinging Cu K $\alpha$  radiation by about a factor of 3.7 on transmission. This is known as the film factor. It was not necessary to assume its value, since it was always possible to measure some reflections on both the first and the second films, and others on both the second and the third films, by means of an intensity strip. The intensity strip (or intensity standard) was prepared by choosing a strong reflection (for the purpose of reducing the time necessary for its preparation) and exposing it many times side by side on the same

film for varying exposure times. The relative intensity of the spots so produced was assumed to be proportional to the exposure time. The strip was prepared so that adjacent spots always had the same ratios of intensity. This gives the impression of equal increments of blackness from the weakest to the strongest spot, since the sensitivity of the eye is roughly proportional to the logarithm of the amount of blackening.

Intensities from the following six Weissenberg photographs were measured:  $(hk0)$ ,  $(hk1)$ ,  $(hk3)$ ,  $(hk5)$ ,  $(h0l)$ , and  $(h2l)$ . The number of intensities which were measured and recorded from these pictures was about 475. This constitutes about half of the measurable data from copper  $K\alpha$  radiation. The final refinement of the structure parameters was carried out by least squares methods which do not require complete data. There were good reasons for the selection of the particular data enumerated above. It was recognized early from the unit cell dimensions and the space group that a half cell Fourier projection onto  $(001)$  would be useful for the initial determination of semi-refined  $x$  and  $y$ -parameters. For this purpose the equatorial and odd layer lines around  $c_0$  are required. The  $(h0l)$  reflections were required for Patterson and Fourier projections onto  $(010)$ , which were useful in the determination of the trial structure. The  $(h2l)$  photograph was taken because it contains some reflections in common with all of the layer lines around  $c_0$ , and

could therefore be used to determine the relative scale factors for the different layer line photographs around  $c_0$ . (The  $(h0l)$  photograph, due to space group extinctions, has no reflections in common with the odd layer lines around  $c_0$ .)

All observed intensities were corrected by the inverse Lorentz and polarization factors. This correction has the formula

$$\frac{\sin 2\theta}{1 + \cos^2 2\theta} \sqrt{1 - \frac{\sin^2 \mu}{\sin^2 \theta}}$$

for equi-inclination Weissenberg photographs, where  $\theta$  is the Bragg angle and  $\mu$  is the inclination angle. The quantity in the denominator is the polarization factor, the rest the inverse Lorentz factor. Other corrections were assumed to be small enough to be ignored, as is commonly done in the case of organic crystals. The square roots of these corrected intensities were then taken and were assumed to be proportional to the absolute values of the corresponding structure factors.

#### Experimental work on ammonium picrate

With some exceptions which will be detailed here, most of the experimental work so far described for potassium picrate was also carried out on ammonium picrate. No crystal was cut and ground and no photographs were taken about any axes other than  $c_0$ . The density was not determined. Pure ammonium picrate is lighter in color than the potassium salt. Its color can be darkened, just as that of potassium picrate, by heating in an excess of ammonium hydroxide.

## UNIT CELL AND SPACE GROUP DETERMINATION

### The Approximate Unit Cell Dimensions

The approximate value of  $c_0$  was found to be  $7.13 \text{ \AA}$  by measurement of the distance between layer lines in oscillation photographs around  $c_0$ . By combining this value with the axial ratios listed in Groth<sup>(9)</sup>, the approximate values of  $13.3$  and  $19.1 \text{ \AA}$  were obtained for the  $a_0$  and  $b_0$  axes, respectively. These values were sufficiently accurate for the purpose of indexing all photographs.

### Accurate Unit Cell Dimensions

The  $a_0$  and  $c_0$  axes were determined from the single film ( $h0l$ ) Weissenberg picture previously described. Film shrinkage corrections were made by means of fiduciary marks placed on the undeveloped film. The distance between these marks on the developed film and the distances of all reflections from the center of the film were measured on a traveling microscope. The best values for  $a_0$  and  $c_0$  were determined from these measurements by a method of least squares which will now be described.

The equation for the  $\theta$  coordinate of a ( $h0l$ ) reflection is  $h^2a^{*2} + l^2c^{*2} = 4(\sin^2\theta)/\lambda^2$ , where  $a^*$  and  $c^*$  are the reciprocal  $a_0$  and  $c_0$  axes, respectively, and  $\theta$  is measured directly from the film. The angle  $\theta$  is the Bragg angle and is equal to one-half of the angle between the incident and the diffracted beams. In radians  $\theta$  is equal to  $y_{\text{corr.}}/2r$ , where  $r$  is the camera radius and  $y_{\text{corr.}}$  is the distance

along the circular cross section of the cylindrical film between the reflection and the undiffracted beam. The subscript "corr." indicates that the measured distance has been corrected for film shrinkage. The position of the undiffracted beam is determined by the presence of symmetrically equivalent spots in the upper and lower halves of the film. Let  $Q = 4(\sin^2\theta)/\lambda^2$ . We therefore obtain an observational equation of the type  $h^2a^2 + \ell^2c^2 = Q$  for the measurement of each  $(h0\ell)$  reflection. The next step in the least squares procedure is to multiply each observational equation by the square root of its weight. This weight,  $w$ , is proportional to the reciprocal square of the expected error in  $Q$ . The error in  $Q$

$$\Delta Q = \frac{dQ}{d\theta} \Delta \theta = 4/\lambda^2(\sin 2\theta) \Delta \theta.$$

The quantity  $\Delta \theta$  can be presumed constant over the whole film since it is proportional to the error in the measurement of distances from the center of the film. We find therefore, that  $\Delta Q \propto (\sin 2\theta)/\lambda^2$ , and  $\sqrt{w} \propto \lambda^2/\sin 2\theta$ , where  $\lambda$  is the wave length. Forty-five weighted observational equations were then reduced to two normal equations in the unknowns  $a^2$  and  $c^2$  by well known methods, described, for instance, in Whittaker and Robinson<sup>(12)</sup>. The solutions of these two simultaneous linear equations yielded the best values of the squares of the reciprocal  $a$  and  $c$  axes. The probable errors of these quantities were also calculated by formulae given

in the above reference. These were then converted into the values for the real axes and their probable errors. The resulting values are:  $a_0 = 13.332 \pm 0.002 \text{ \AA}$ ,  $c_0 = 7.154 \pm 0.001 \text{ \AA}$ . The values for these parameters depend on the following assumed values for the various wave lengths used:  $\text{Cu K}\beta = 1.3921 \text{ \AA}$ ,  $\text{Cu K}\alpha_1 = 1.5405 \text{ \AA}$  and  $\text{Cu K}\alpha_2 = 1.5443 \text{ \AA}$ . In the region where the  $\alpha_1 - \alpha_2$  doublet is not resolved, the weighted average value of  $\text{Cu K}\alpha = 1.5418 \text{ \AA}$  was used.

A similar determination of  $a_0$  and  $b_0$  was made by the use of oscillation photographs taken around the  $c_0$  axis. Since these were taken in a larger, 5 cm radius camera, the positions of the reflections could be measured with satisfactory accuracy with a brass vernier scale. Only ten reflections were measured and only ten observational equations were used. The system of weighting was the same as before. The following results, with their probable errors, were obtained:  $a_0 = 13.327 \pm 0.004$  and  $b_0 = 19.160 \pm 0.006 \text{ \AA}$ . The probable errors in this determination are naturally higher, but the value for  $a_0$  checks satisfactorily with the one previously obtained.

As the result of these two determinations, the following values were adopted for the unit cell constants:  $a_0 = 13.33 \pm 0.01 \text{ \AA}$ ,  $b_0 = 19.16 \pm 0.02 \text{ \AA}$ , and  $c_0 = 7.154 \pm 0.005 \text{ \AA}$ . The error limits are equal to about three times the probable errors.

Determination of the Space Group

The observed Laue symmetry of potassium picrate is  $D_{2h} - mmm$ . This fact merely puts the crystal in the orthorhombic system. The following extinctions were observed after the Weissenberg photographs had been indexed:

- (a):  $(hkl)$  when  $(h + k + l)$  is odd
- (b):  $(hk0)$  when either  $h$  or  $k$  is odd
- (c):  $(h0l)$  when  $h$  or  $l$  is odd
- (d):  $\left. \begin{array}{l} (hkl) \\ (hk3) \\ (hk5) \end{array} \right\}$  when either  $h$  or  $k$  equals zero.

No  $(0kl)$  Weissenberg photograph was taken, but from (a) and (d) it is clear that those  $(0kl)$  reflections are absent for which either  $k$  or  $l$  is odd. These extinctions lead unambiguously to the space group  $D_{2h}^{27} - I_{bca}$ .

Space Group Requirements

A drawing of the space group is given on page 74. It makes use of the same conventions as those adopted in the Internationale Tabellen<sup>(13)</sup>, and, in fact, our diagram looks identical to that given in the tables. There is a difference, however, in that our choice of labeling the axes corresponds to an exchange of the  $a_0$  and  $b_0$  axes from the illustration in the Internationale Tabellen. The result of this is that our quantity  $A$ , from which the structure factors are calculated, is different from the  $A$  listed in the tables. Our quantity has the formula

$$A = 16 \cos \frac{2\pi(h+k+l)}{4} \cos 2\pi(hx + k/4) \cos 2\pi(ky + l/4) \cos 2\pi(lz + h/4)$$

The A listed in the tables is obtained from ours by interchanging x and y as well as h and k. The general position in this space group is 16-fold and can be expressed as

$$000, \frac{1}{2}\frac{1}{2}\frac{1}{2}, \frac{1}{2} \quad (xyz; x, \bar{y}, z+\frac{1}{2}; x+\frac{1}{2}, y, \bar{z}; \bar{x}, y+\frac{1}{2}, z)$$

in terms of our axes. The special positions will be described in the next section.

### The Number of Molecules per Unit Cell

The number of molecules per unit cell was calculated from the experimentally measured density, the known molecular weight, and the volume of the unit cell as determined by the measured lattice constants. The measured density was 1.940 g/cc. These are thus  $7.986 \sim 8$  molecules per unit cell. The density reported in Groth<sup>(9)</sup> is 1.852 which is undoubtedly too low. Since the general position in this space group is 16-fold both the potassium and the picrate ions must be in special positions. A reference to the space group diagram, Figure 7d, page 74, shows that the only kinds of special positions there are lie on centers of symmetry and two-fold axes. There are two independent sets of centers and three independent sets of two-fold axes. The potassium ion could be in any one of these special positions, but the picrate ion cannot have a center of symmetry and must therefore be on one of the three sets of axes.

DETERMINATION OF THE TRIAL STRUCTURE

It was first planned to determine the trial structure by the isomorphous replacement technique, working simultaneously with ammonium and potassium picrate. The first step was an attempt to find the position of the potassium atom. For this purpose the values of  $F^2(hk0)$  of both salts were used to prepare Patterson projections. The Patterson projection of the potassium salt showed a very high and elongated peak at  $u = \frac{1}{4}$ ,  $v = 0$ , the elongation being in the  $u$  direction. In Patterson space  $u$ ,  $v$ , and  $w$  correspond to  $x$ ,  $y$ , and  $z$  in Fourier space. From the height of this peak, it was felt that it must contain a potassium-potassium interaction, along with other interactions. This was substantiated by the appearance of the Patterson projection of ammonium picrate, in which there is a smaller peak at  $u \cong 1/6$ ,  $v = 0$  and a corresponding one, required by symmetry, at  $u \cong 1/2 - 1/6 = 1/3$ ,  $v = 0$ . (The space group symmetry of the projections demands that the lines  $u = \frac{1}{4}$  and  $v = \frac{1}{4}$  are mirror lines; the asymmetric unit of the projection is contained in the region  $u = 0$  to  $\frac{1}{4}$ ,  $v = 0$  to  $\frac{1}{4}$ .) It was concluded that the valley between the two medium sized peaks in the projection of the ammonium salt was being filled in by two large potassium-potassium peaks at  $u = \frac{1}{4} - \Delta$ ,  $v = 0$  and  $u = \frac{1}{4} + \Delta$ ,  $v = 0$  in the case of the potassium salt. The quantity  $\Delta$  would have to be small enough so that the superposition of the two potassium peaks would yield a maximum density at  $u = \frac{1}{4}$ .  $\Delta$  could be zero, of course, in which case

the two potassium-potassium peaks would be exactly superimposed. Now the potassium atom must be in special positions, since there are only eight of them in the unit cell, whereas the general position is sixteen-fold. They could be at either one of two sets of centers of symmetry (see space group diagram, p.74 ), or somewhere along any one of three sets of two-fold axes. The Patterson projection indicated that the potassium atom in the asymmetric unit is located on the two-fold axis parallel to  $a_0$  with a y-coordinate of  $\frac{1}{4}$  and an x-coordinate of  $x = 1/8 \pm \Delta/2$ . There would then have to be another one at  $y = \frac{1}{4}$ ,  $x = -1/8 \pm \Delta/2$ , resulting in an inter-potassium vector with a zero y-component and an x-component of  $1/4 \pm \Delta$ , thus explaining the Patterson peak at  $u = 1/4 \pm \Delta$ .

From considerations involving the expected half width of a potassium-potassium Patterson peak, the quantity  $\Delta$  could be as high as  $0.04 a_0$ . The x-parameter of potassium could therefore be anywhere in the region  $.105 \leq x \leq .145$ , i.e.  $1/8 - \Delta/2 \leq x \leq 1/8 + \Delta/2$ . This uncertainty was too large to calculate with any accuracy the contribution of the potassium atom to the structure factors and thereby determine their signs. There were other difficulties with regard to the use of the isomorphous replacement technique. For instance, since the x-parameter for the potassium atom is close to  $1/8$ , this atom would not contribute much to reflections in the  $(hk0)$  zone for which  $h = 4n + 2$ , since the formula for  $F(hk0)$  involves a factor of  $\cos 2\pi hx$ . There would be many other reflections

whose structure factors contain only a small contribution from the potassium because the scattering power of the latter is quite small compared to the combined scattering power of the picrate ion. The ratio is 18:116 at zero scattering angle, and becomes somewhat more favorable for the potassium atom with increasing scattering angle. Although the waves from the various atoms in the picrate ion never reinforce fully, there are some structure factors to which the picrate ion makes a strong contribution whereas the potassium atom frequently does not contribute with its full weight, as we have seen, because of interference with its own symmetry counterparts. In short, the potassium is not quite heavy enough and is not located favorably enough to make the method of isomorphous replacement very useful in this investigation.

There was also some doubt as to whether potassium picrate and ammonium picrate are actually strictly isomorphous. The (hk0) Patterson projections of the two showed some similarity but also some important differences, other than the potassium-potassium interaction. The differences might, of course, have been due to interactions of the potassium atom with other atoms, but there was no way to check on this question at this stage of the investigation. On the basis of the final results for potassium picrate this point can now be cleared up to some extent. From the final set of parameters for potassium picrate, a set of structure factors  $F(hk0)$  were calculated by substituting a nitrogen atom for the potassium atom. These were then compared with the observed structure

factors for ammonium picrate. A rough scale and temperature factor were determined statistically and the reliability factor was then calculated. This factor was 28% for the 81 values of  $F(hk0)$  used in the calculation. The value of 28% is so low that there must be a great deal of similarity between the two structures. Nevertheless the two structures cannot be completely identical, since the reliability factor for potassium picrate, calculated from the same parameters, is much lower.

The next step in the attempt to find the correct trial structure was a series of trial and error calculations on both the potassium and the ammonium salts. These calculations consisted of trying out various reasonable models and comparing structure factors calculated from these models with the observed structure factors. Structure factors having low Bragg angles were used for this purpose since these are least sensitive to the exact values of the parameters. Several space group considerations could be used to limit the number of possible variables in this procedure. The picrate ion must lie on a two-fold axis, as has been pointed out before, and this axis must accommodate two picrate ions in a row. From stereochemical principles it is clear that two such picrates in a row would need a linear dimension of at least about 18 Angstroms. It is necessary, therefore, that these ions must lie on the two-fold axes parallel to  $b_0$ , whose length is  $19.16 \overset{\circ}{\text{A}}$ . Now the picrate molecule is a relatively rigid affair whose geometry can be roughly predicted from structural chemical principles with sufficient

accuracy for the determination of a trial structure. About the only aspect of the molecule which cannot be predicted easily is the kind and degree of deformation of the ortho nitro groups due to steric hindrance between the phenol oxygen and one of the oxygens in the nitro group. Its position and orientation in the unit cell are subject to only two variables -- the position of the ion as whole along the two-fold axis and the angle of rotation around the axis. In addition to these two variables, there remained the uncertainty with regard to the exact position of the potassium ion on the two-fold axis parallel to  $a_0$ . This third variable is the x-parameter of the potassium ion, which was correctly suspected to be somewhere near  $1/8$ . These three variables, then, were the only ones subject to large uncertainties. They were the only ones which needed to be found by trial and error to determine an approximate trial structure, which could then be refined by routine numerical calculation techniques.

This purely trial and error method failed because of an additional, and, as it turned out, unjustified assumption which was made. It was assumed that the angle of rotation of the picrate ion around its two-fold axis need not be determined experimentally, but that it could be assumed to be small relative to (001), i.e. that the plane of the benzene ring must be nearly parallel to the crystallographic plane (001). Angles of tip of  $0^\circ$ ,  $5^\circ$ , or at most  $10^\circ$  were tried at various times. The x-parameter of potassium was then

determined by calculating the structure factors for the (h00) reflections as a function of this parameter and picking out the value which gave the best fit with the observed structure factors. It was possible to get reasonable fits for the (h00) reflections in this manner, but the agreement was fortuitous, leading to an incorrect potassium parameter which somehow compensated for the wrong angle of tip of the benzene ring. The y-parameter of the picrate ion was obtained by calculating values for (0k0) structure factors; these are independent of the other two trial parameters. With these values for the trial parameters, a few general (hk0) structure factors were calculated and these never showed any agreement with the observed values. Several unsuccessful calculations of this type were carried out, using different models for the rigid picrate ion, particularly varying the dihedral angle between the ortho nitro group and the benzene ring.

There were two good reasons for the incorrect assumption that the benzene rings should be nearly parallel to (001). In the first place, the short  $c_0$  axis of  $7.15 \text{ \AA}$  has to accommodate two layers of picrate ions, which are situated on two-fold axes separated by  $3.58 \text{ \AA}$ . The more the ions are tilted around these axes, the shorter the perpendicular distance between the planes of the two picrate ions will become. It was later determined, however, that the angle of tip is  $22^\circ$ , a value which leads to some intermolecular distances shorter than normal. The other reason

concerned the optical data listed in Groth<sup>(9)</sup>, where it is stated that the birefringence is negative and the indices of refraction for light vibrating parallel to  $a_0$  and for light vibrating parallel to  $b_0$  are nearly equal. In fact, they cross over in the visible. Now if there were a large angle of tip of the picrate ion, one would expect the index for light with the electric vector parallel to  $b_0$  (i.e. the two-fold axis of the picrate) to be materially larger than that for light vibrating parallel to  $a_0$  with only a component in the plane of the benzene. The reason for the optical behavior is not clear in view of the final structure.

Eventually larger angles of tip would probably have been tried, but first a new approach was attempted which led to the correct trial structure. At about this time it was learned that the group of investigators at Johns Hopkins University were working on ammonium picrate. All subsequent effort was therefore concentrated on the potassium salt. A crystal was cut and ground as previously described and a  $(h0l)$  Weissenberg was taken by rotating the crystal around the  $b_0$  axis. From the intensities of the  $(h0l)$  reflections a Patterson projection onto  $(010)$  was made. This is shown in Figure 1. As an aid to the interpretation of this Patterson projection, let us first consider the asymmetric unit of the projection of the structure onto  $(010)$ , Figure 2, which was made from the final and most accurate set of parameters. Figure 6, page 65, shows the labeling of the atoms in a

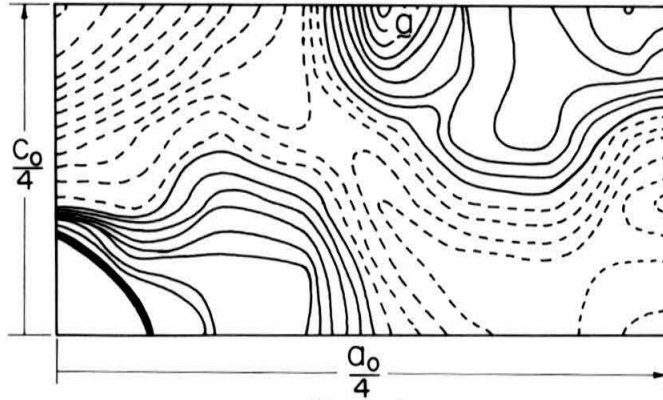


Figure 1  
(h0l) Patterson, broken lines indicate negative contours. Arbitrary interval. Contours at the origin are omitted.

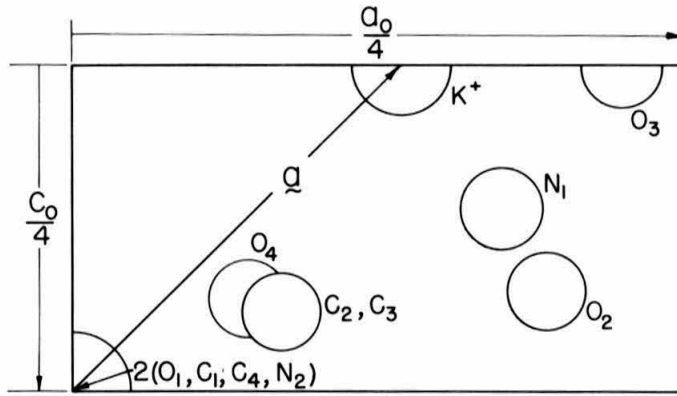


Figure 2  
Projection of molecule onto (010) from final parameters

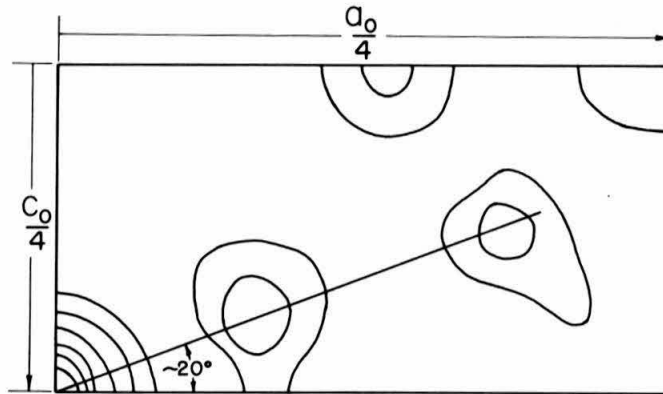


Figure 3  
First (h0l) Fourier with arbitrary contour intervals

picrate ion which has been adopted; the primed atoms are related to the corresponding unprimed atoms by the two-fold axis through atoms,  $O_1$ ,  $C_1$ ,  $C_4$ , and  $N_2$ . Figure 2 can be understood if we imagine the two-fold axis of the molecule perpendicular to the plane of the paper at the point  $x = 0$ ,  $z = \frac{1}{4}$ . All of the unprimed atoms will then project into the 1/16th of the unit cell shown, which is the asymmetric unit of the projection. The primed atoms will project into another 1/16th, not shown. The atoms  $O_1$ ,  $C_1$ ,  $C_4$ , and  $N_2$ , all lying on the two-fold axis of the molecule, will project on top of each other onto the point  $x = 0$ ,  $z = \frac{1}{4}$ . These four atoms will be referred to as the "special position atoms" in the following discussion. Behind the molecule in question there is required to be another one, on the same two-fold axis. Its special position atoms also project onto the point  $x = 0$ ,  $z = \frac{1}{4}$ , while the rest of its atoms project into other 1/16th sections of the unit cell not shown, because this second molecule must be tipped in the opposite direction relative to the (001) plane. The point  $(0, \frac{1}{4})$  therefore contains the superposed projection of eight atoms, 4 carbons, two nitrogens, and two oxygens, with a total of 54 electrons. This feature is required by the space group and was known before the Patterson projection was interpreted. It was therefore expected that there would be a strong Patterson peak corresponding to the interaction between these eight atoms and the potassium ion as indicated by the vector  $\underline{g}$  in Figure 2.

The potassium ion was believed to be at  $z = 0$  and  $x =$  about  $1/8$ . The Patterson peak would therefore be expected along the line  $w = \frac{1}{4}$  somewhere near  $u = 1/8$ . There is indeed a high peak at  $w = \frac{1}{4}$ ,  $u = 0.133$  (labeled  $g$  in Figure 1) which was ascribed to the interaction between the potassium ion and the atoms in special positions of the picrate ion. But there is another peak, almost as high, at  $w = \frac{1}{4}$  and  $u =$  nearly  $\frac{1}{4}$ . This peak is due to the interaction between the special position atoms of the picrate ion and one of the oxygens of type  $O_3$ , as can be verified from Figure 2. This fact was not realized at the time, and it was concluded instead that the potassium ions are randomly distributed between either one of two positions, i.e. mostly at  $x = 0.133$  and to a lesser extent at  $x \cong 0.250$ . Another (correct) conclusion which was drawn from the Patterson projection was that the benzene rings could not be nearly parallel to (001). If they were, the structure would be very layerlike and this would be reflected in the Patterson projection by a layer of high density all along the line  $w = 0$ . Actually some of the lowest density is along this line, while the region of highest density stretches diagonally across the Patterson projection. This indicates an angle between the benzene ring and (001) which might be as high as perhaps  $27^\circ$ . A compromise guess of  $20^\circ$  was made and this value was later shown to be nearly correct. With these conclusions from the Patterson projection, a set of  $(h0\ell)$  structure factors was calculated and their signs were used to make a Fourier projection down  $b_0$ , shown in Figure 3. The interpretation of this projection was obvious and showed that the potassium

ions are not randomly distributed, but instead have the definite x-parameter of about 0.133. It also confirmed the guess that the angle of tilt of the benzene ring relative to (001) is about  $20^\circ$ . The atoms  $C_2$ ,  $C_3$ , and  $O_4$  are nearly superimposed in this projection, as is to be expected, and cause a large, diffuse peak. The atom  $N_1$  is not well resolved from atom  $O_2$ , and atom  $O_3$  is unresolved from its own symmetry counterparts. The positions of the atoms were adjusted on the basis of this projection, and new structure factors  $F(h0\ell)$  were calculated. A second  $(h0\ell)$  Fourier projection was then calculated, but it did not yield much additional accuracy or detailed information.

Two of the three important trial parameters, the angle of tip of the benzene ring and the position of the potassium atom had now been found. It remained to find the third parameter, namely the y-parameter of the picrate ion as a whole. This was done by a trial and error procedure. A few  $(hk0)$  structure factors having low Bragg angles were calculated for various values of the picrate ion y-parameter and were plotted against the latter. There was only one value of the argument for which the relative heights of the different curves agreed approximately with the corresponding observed structure factors.

A trial structure had now been found. The next step consisted of calculating all the  $(hk0)$  structure factors and making an  $(hk0)$  Fourier projection. This projection was quite informative, showing considerable detail. The potassium ion appeared with the same x-parameter as in the  $(h0\ell)$

projection. The atoms  $O_1$ ,  $C_2$ ,  $N_1$ ,  $O_2$ ,  $C_4$ , and  $O_4$  were fairly well resolved. The other atoms were partially or completely unresolved due to superposition with atoms from the molecules in the layer below, or due to a fusion with their own symmetry counterparts across the mirror lines bounding the asymmetric unit of the projection. An improved model for the structure was formulated from the information obtained from the first (hk0) Fourier. From the new model a second (hk0) Fourier was calculated in order to obtain further improvement of those parameters which are resolved on this projection.

## THE REFINEMENT OF THE STRUCTURE

### Determination of Scale and Temperature Factors

It has been previously mentioned that when the intensities of reflections are corrected by the inverse Lorentz and Polarization factors, the square roots of the corrected intensities are proportional to the structure factors:

$$\sqrt{I_{\text{corr.}}} = \frac{1}{K} |F| \times \text{temperature factor}; \quad F = \sum_i f_i A_i.$$

Here  $F$  is the temperature independent part of the structure factor; the summation extends over all the atoms in the asymmetric unit of the unit cell;  $f_i$  are the atomic scattering factors (or form factors) which are a function of the Bragg angle for the reflection in question and are listed for all the atoms in tabular numerical form in "Internationale Tabellen..."<sup>(13)</sup>; The quantity  $A_i$  for this space group has already

been defined on page 15 . The temperature factor will be discussed in detail later.  $K$  is the scale factor, which is different for each film since the intensities for each film are measured on an arbitrary scale. The usual procedure is to determine the relative scale factors for the different photographs experimentally, bringing all observed structure factors to the same scale, and then to determine one absolute scale factor by statistical methods involving the comparison of a large number of observed and calculated structure factors. For the purpose of determining the relative scale factors, the (h2 $\ell$ ) Weissenberg photograph had been taken. This contains the (h20) reflections in common with the zero layer photograph around  $c_0$ , the (h21) reflections in common with the first layer, the (h23) reflections in common with the third layer, and the (h25) reflections in common with the fifth layer around  $c_0$ . The (h0 $\ell$ ) photograph contains the (h00) reflections in common with the zero layer around  $c_0$ . In principle, therefore, the relative scale factors could have been determined from the collected experimental data. Actually the number of reflections which could be observed on both of any two photographs was so small, only about five, that the average deviations of the relative scale factors so obtained were too large. This situation arises because any single visually determined  $F$  value is liable to be in error by about 10%, so that the ratio of two independent estimations of a single  $F$  may be considerably in error. Consequently the average of many ratios is needed to obtain sufficiently accurate relative scale factors. With complete data, collected from photographs

taken with the crystal rotated about all three axes, it would have been possible to determine satisfactory scale factors but in our case it was not. To obtain greater accuracy in scale factors it was therefore decided to determine the absolute scale factor for each of the six photographs separately, by means of a statistical comparison of calculated and observed structure factors.

The temperature factor used in this investigation is an anisotropic three parameter factor of the form

$$e^{-(\alpha h^2 + \beta k^2 + \gamma l^2)}.$$

A factor of this form is by no means theoretically adequate, but it is better than the one-parameter isotropic factor frequently used. It is also the most complicated form which can be used without enormously increasing the expense and complexity of the already time consuming and costly numerical calculations which went into the refinement of this structure. It leads to the following relation between observed and calculated structure factors:

$$K_j |F_{\text{obs}}| = |F_{\text{calc}}| e^{-(\alpha h^2 + \beta k^2 + \gamma l^2)} \quad \text{and}$$

$$\ln K_j + \alpha h^2 + \beta k^2 + \gamma l^2 = \ln \frac{|F_{\text{calc}}|}{|F_{\text{obs}}|}$$

The subscript  $j$  takes the values 1 to 6, for the six different films from which intensity data were collected. The logarithmic equation is linear in the unknowns, which are the  $\ln K_j$ 's,  $\alpha$ ,  $\beta$ , and  $\gamma$ . An equation of this type can be

written for each of the 475 reflections for which  $F$  was observed and calculated. Each equation should be weighted by the reciprocal square of the expected absolute error in the quantity on the right of the logarithmic equation. The expected error is equal to the square root of the sum of the squares of the percentage errors in  $F_{\text{calc}}$  and  $F_{\text{obs}}$ . The percentage error in  $F_{\text{obs}}$  is roughly constant except for very weak reflections, and its value can be estimated from the reproducibility of intensity measurements. The expected percentage error in  $F_{\text{calc}}$  is probably roughly proportional to  $1/F_{\text{calc}}$  within narrow regions of  $\sin \theta$ , and increases with increasing Bragg angle. Since the error in  $F_{\text{calc}}$  cannot be easily estimated, only those equations were used for which  $F_{\text{calc}}$  was sufficiently large to insure a reasonably small percentage error. These equations were then all given unit weight. This procedure was followed in the first temperature and scale factor least squares procedure of this type. After rejecting the equations for which  $F_{\text{calc}}$  was too small, 136 equations remained. These were reduced to nine normal equations in the nine unknowns -- six scale factors and three temperature parameters -- by well known methods. This procedure was carried out before the first least squares refinement in the space parameters, described in a later section, since accurate scale and temperature factors were needed in this type of refinement.

With a more accurate set of calculated structure factors, based on the results of the first space parameter least squares

refinement, a second and final scale and temperature factor determination was carried out. This time a crude system of weighting was used by making rough estimates of the error in the calculated values of  $F(hk\ell)$ . The set of calculated values of  $F(hk\ell)$  were, of course, more reliable than the previously used set. In spite of these two changes the resulting values for the scale and temperature factors did not differ significantly from the values obtained in the first determination. The following values were adopted for the three temperature factor parameters and were used in the last two stages of the refinement of the structure:

$$\alpha = 0.0027, \quad \beta = 0.0014, \quad \gamma = 0.0124$$

These values correspond to mean square displacements of all the atoms from their equilibrium positions of about  $0.024 \text{ \AA}^2$  in the  $a_0$  direction,  $0.026 \text{ \AA}^2$  in the  $b_0$  direction, and  $0.032 \text{ \AA}^2$  in the  $c_0$  direction. The estimated errors are about 10 or 15%, so that the mean square amplitudes of vibration in the  $a_0$  and  $b_0$  directions are equal within experimental error, while those in the  $c_0$  direction are somewhat larger. In terms of the isotropic temperature parameter  $B$  which is frequently used,  $\alpha$ ,  $\beta$ , and  $\gamma$  correspond to  $B \approx 2.0$  for  $(hk0)$  reflections and  $B \approx 2.5$  for  $(00\ell)$  reflections.

#### The Half-cell Fourier Projection onto (001)

The first step in the refinement of the trial structure was a half cell Fourier projection onto (001). All picrate

ions were known to lie on two-fold axes with z-parameters of either  $z = 1/4$  or  $z = 3/4$ . Although they are all tipped by  $22^\circ$  relative to (001), this angle is easily small enough for a projection of a single molecule onto (001) to be resolved. However, we have seen that a full cell (hk0) projection suffers from a considerable amount of overlap between one molecule centered at  $z = 1/4$  and another at  $z = 3/4$ . A half-cell projection which projects only the contents of the unit cell bounded between the planes  $z = 1/2$  and  $z = 0$  would obviate this difficulty by showing the projection of only one molecule. A set of relatively accurate x- and y -- parameters of all the atoms could be determined in this way.

The electron density for this space group, with the particular choice of origin and axes we have made, can be expressed as:

$$\begin{aligned}
 (1) \quad \rho(xyz) = & \frac{8}{V} \left[ \sum_0^\infty \sum_{k=2n}^{\infty} F_{hke} \cos 2\pi hx \cos 2\pi ky \cos 2\pi lz \right. \\
 & - \sum_0^\infty \sum_{k=2n+1}^{\infty} F_{hke} \sin 2\pi hx \cos 2\pi ky \sin 2\pi lz \\
 & - \sum_0^\infty \sum_{k=2n+1}^{\infty} F_{hke} \sin 2\pi hx \sin 2\pi ky \cos 2\pi lz \\
 & \left. - \sum_0^\infty \sum_{k=2n}^{\infty} F_{hke} \cos 2\pi hx \sin 2\pi ky \sin 2\pi lz \right]
 \end{aligned}$$

Let us denote the half-cell projection density as  $\sigma_{\frac{1}{2}}(x,y)$ .

$$\begin{aligned}
 (2) \quad \sigma_{\frac{1}{2}}(x,y) = & \int_0^{\frac{1}{2}} \rho(x,y,z) dz \\
 = & 8/V \left[ \frac{1}{2} \sum_0^\infty \sum_{k=2n}^{\infty} F_{hko} \cos 2\pi hx \cos 2\pi ky \right. \\
 & \left. - \sum_{l=2n+1}^{\infty} \frac{1}{\pi l} \sum_0^\infty \sum_{k=2n}^{\infty} F_{hke} \cos 2\pi hx \sin 2\pi ky \right]
 \end{aligned}$$

Equation (2) shows why only the F values for reflections with  $\ell = 0$  or  $2n + 1$  are required for the half-cell projection. The first term contains only the values of  $F(hk0)$ , while the second contains the summation over odd  $\ell$  as well as the double sum over  $h$  and  $k$ . In fact, only half of the data from each odd layer are used. The  $(hk\ell)$  combinations for which  $h = 2n$  and  $k = 2n + 1$  are omitted. On the other hand, formula (2) requires a summation over all values of  $\ell$  from zero to infinity. Actually, the highest value of  $\ell$  for which all data had been collected was  $\ell = 5$ , from the 5th layerline photograph around  $c_0$ . The question then was what to expect from such a non-ideal series, terminated after  $\ell = 5$ . This point will be discussed in some detail because such a discussion has not been found in the literature\*.

The expression for the half-cell projection  $\sigma_{\frac{1}{2}}^{\frac{1}{2}}(x,y)$  can alternatively be formulated as

$$(3) \quad \sigma_{\frac{1}{2}}^{\frac{1}{2}}(x,y) = \int_0^1 w(z) \rho(xyz) dz$$

Here the integration is over the whole range of  $z$ , but the weighting function  $w(z)$  is a step function which gives unit weight to the integrand in the region  $0 \leq z \leq \frac{1}{2}$  and zero weight in the region  $\frac{1}{2} \leq z \leq 1$ . The graph for an ideal  $w(z)$  is shown by the solid line in Figure 4. Its Fourier

-----  
 \* The following discussion is based on conversations with Drs. E. W. Hughes and V. Schomaker, who kindly clarified this matter for me.

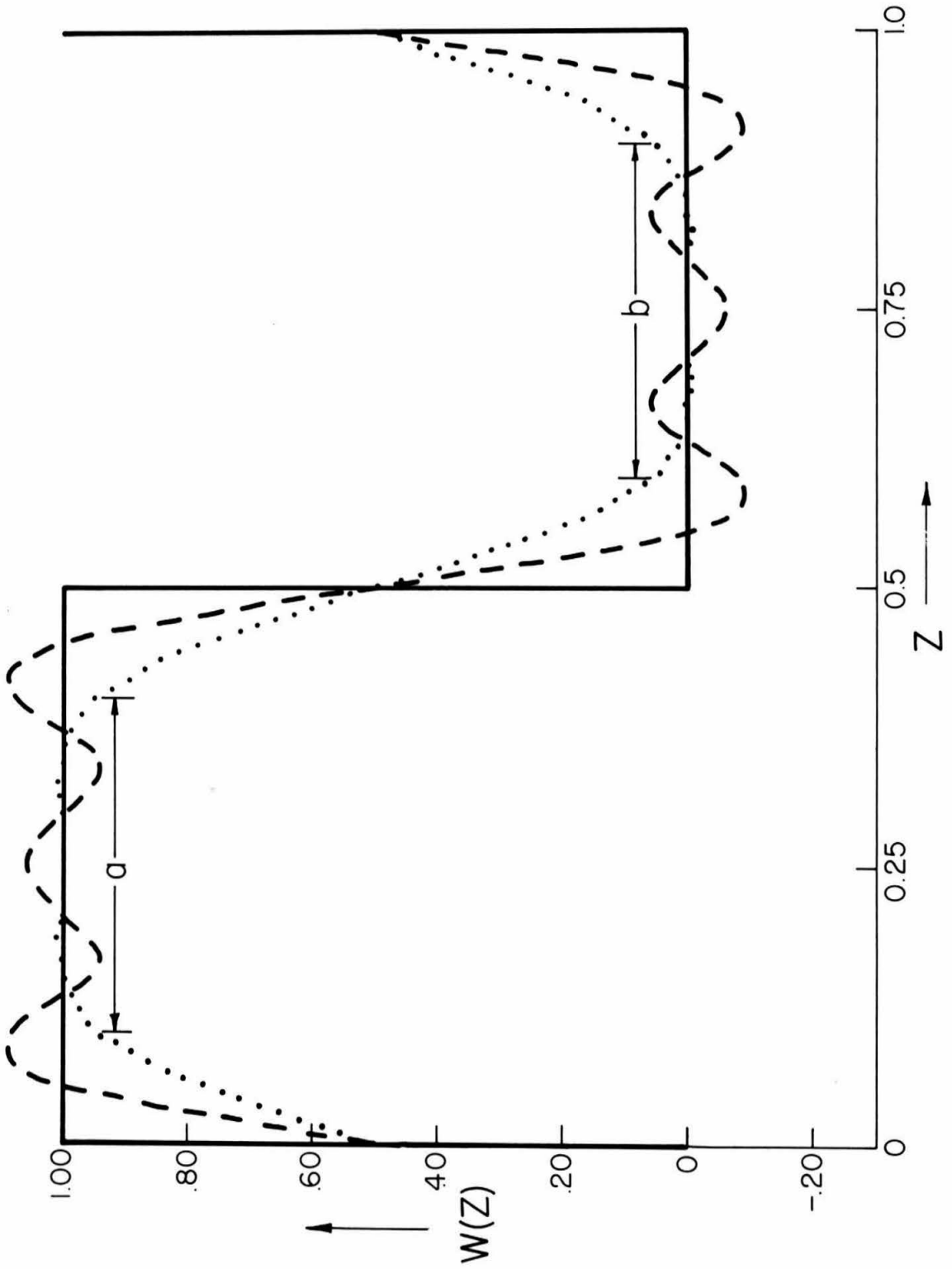


Figure 4

representation is

$$(4) \quad w(z) = \frac{1}{2} + \sum_{\substack{n=1 \\ \text{odd } n \text{ only}}}^{\infty} (2/\pi n) \sin 2\pi n z$$

If (4) and (1) are explicitly put into (3) and the implied integration is carried out, the result becomes identical to (2), as it must. Now let us consider an imperfect weighting function of the form

$$(5) \quad w'(z) = A_0 + A_1 \sin 2\pi z + A_3 \sin 6\pi z + A_5 \sin 10\pi z$$

Inserting (5) into (3) and integrating, we obtain

$$(6) \quad \sigma_0'^{\frac{1}{2}}(x,y) = A_0 \sum_0^{\infty} \sum_0^{\infty} F_{hko} \cos 2\pi h x \cos 2\pi k y \\ - \sum_{\substack{\ell=1,3 \\ \text{and } 5}} A_{\ell}/2 \sum_k^{\infty} \sum_{\substack{h=2k+1 \\ k=2k}} F_{hke} \cos 2\pi h x \sin 2\pi k y$$

Equation (6) calls for data from up to and including the fifth layer around  $c_0$  only. These are the data which was available. We conclude that a non-ideal half cell projection made with only the available data corresponds to the use of weighting function of the type (5). We still have a choice with regard to the values of the  $A_{\ell}$ 's. One obvious choice is to let  $A_0 = 1/2$  and  $A_{\ell} = 2/\ell \pi$ . Then (5) will correspond to the first four terms in (4), and the resulting  $\sigma_0'^{\frac{1}{2}}(x,y)$  will correspond to the ideal function (2) from which all terms of  $\ell > 5$  have been dropped. The shape of this imperfect weighting function is shown by the dashed line in Figure 4. The wiggles in this curve are not very serious. They cause a slight variation in the height of

atomic peaks in the projection, depending on the  $z$  parameter of the atom in question.

An alternative procedure is to smooth out these wiggles by finding appropriate numerical values for the  $A_\ell$ 's. This is the procedure which was actually followed. The  $A_\ell$ 's were determined by the following conditions:  $w'(z)$  must be zero at  $z = 1/4$  and at  $z = 3/4$ . The second and fourth derivatives of  $w'$  must be zero at  $z = 1/4$ . (The odd derivatives are automatically zero.) If the above conditions are satisfied function  $w'$  has unit height at  $z = 1/4$  and is as horizontally flat as possible in this region. This function is shown by the dotted curve in Figure 4. The numerical values of the  $A$ 's turn out to be  $A_0 = 0.500$ ,  $A_1 = 0.586$ ,  $A_3 = 0.098$ , and  $A_5 = 0.012$ . These values were substituted into equation (6) for the imperfect half cell projection.

The dotted curve in Figure 4 shows what limitations to expect in the non-ideal half-cell projection. If all the atoms in the lower half of the unit cell were contained in the region  $0.100 \leq z \leq 0.400$ , indicated by the range  $a$  in Figure 4, the projection should closely resemble an ideal one. The atoms in the lower half of the cell would be given unit weight, and their symmetry counterparts in the upper half, contained in the region  $0.600 \leq z \leq 0.900$ , indicated by range  $b$  in Figure 4, would be given zero weight. On the other hand, the dotted curve shows that atoms which are close to the planes  $z = 0$  and  $z = 1/2$  would get somewhere between half and full weight if in the lower half of the cell, and somewhere between zero and half weight if in the

upper half of the cell.

From the trial structure, it was known with fair certainty that all atoms in the picrate ion except atom  $O_3$  and its symmetry counterparts lie in the region of  $z$  favorable for the half-cell projection. They were expected to show up well in the projection, whereas their symmetry counterparts in the upper half of the cell should be cut off. Atom  $O_3$ , on the other hand, would be expected to show up with only about half weight, whereas its counterparts, which ought to be cut off, would also be expected to show up with about the same weight. This is born out by Figure 5 which shows the half-cell projection. By an unfortunate coincidence  $O_3$  and  $O_3'$  (related by the  $c$ -glide plane at  $x = 1/4$ , see space group diagram, p.74 ) have only a small ( $x$ - $y$ ) separation so that their projections are fused. This made it impossible to measure the  $x$ -parameter of atom  $O_3$  accurately from the projection. All other  $x$ -parameters and all  $y$ -parameters could be obtained with rather good precision. The parameters obtained did suffer somewhat from a few incorrect signs of structure factors and from the termination of the series in  $h$  and  $k$ . In most cases they were within  $0.04 \text{ \AA}$  of the final parameters. Only the  $x$ - and  $y$ -parameters of atom  $O_3$  were in error by a large amount. The reason why the  $y$ -parameter of atom  $O_3$  was in error by as much as  $0.08 \text{ \AA}$  is not clear. The half-cell projection, Figure 5, shows a peak with height of about one electron where the hydrogen would be expected. However, this peak may not have any significance

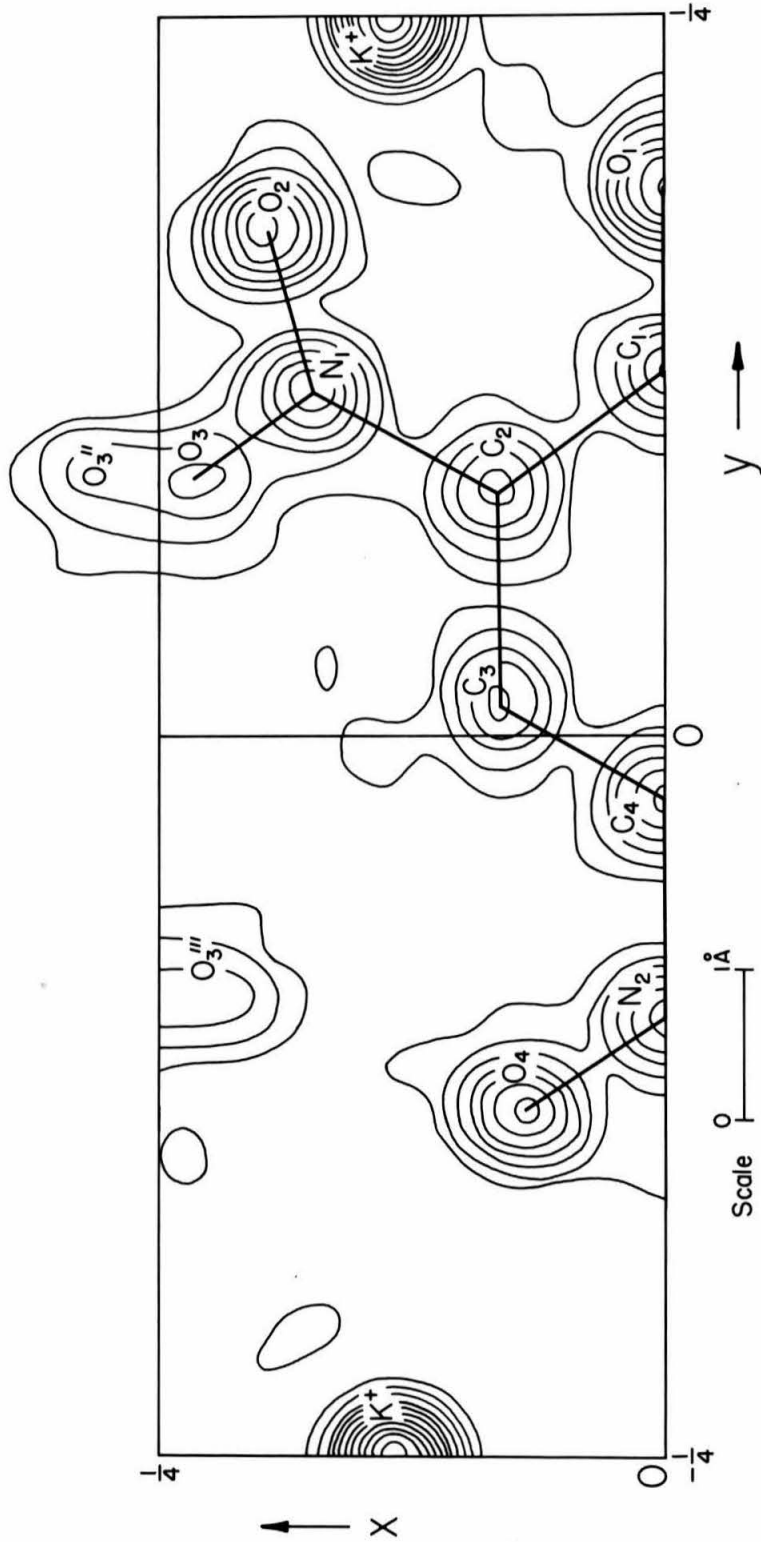


Figure 5  
Half-cell Fourier Projection onto (001)

since the whole one-electron contour is irregular and has several false peaks, mostly in the neighborhood of the potassium atom, as expected.

The following steps were used in calculating the half-cell projection: From the trial model, a set of  $F(hk\ell)$  were calculated, corresponding to the terms needed for the projection. This was done on IBM punched card machines. The signs of the calculated  $F(hk\ell)$  were then combined with the magnitudes of the observed  $F(hk\ell)$  for the evaluation of the series in equation (6). The actual summations were carried out by the use of Beavers-Lipson strips<sup>(14)</sup> and a desk calculator.

#### Refinement of the Structure by Least Squares Methods

Refinement by half-cell projection was not carried beyond the first such projection, shown in Figure 5, because of the limited number of parameters which can be refined by this method. Instead, further refinement was carried out by an application of the method of least squares to the crystal structure problem, as first described by Hughes<sup>(15)</sup>. This method has the advantage that all the collected data can be used and all of the parameters can be refined simultaneously. At the same time it is not necessary to use complete data, or some specific selection of data such as was called for in the half-cell projection. Furthermore, the method is not subject to the errors caused by the termination of ideally infinite series. Such terminations affect the results of Fourier methods unless lengthy corrections are

made for them.

The least squares method as applied in this case will be briefly described. Observational equations of the following type are set up:

$$e^{-(\alpha h^2 + \beta k^2 + \gamma l^2)} \sum_{i=1}^{23} \frac{\partial F(hkl)}{\partial x_i} \Delta x_i = F_{\text{obs}} - F_{\text{calc}} e^{-(\alpha h^2 + \beta k^2 + \gamma l^2)}$$

(hkl)            (hkl)

The summation here is over the 23 different x, y, and z parameters in the asymmetric unit of the structure. There are  $6 \times 3 = 18$  parameters for the six atoms in general positions, plus 5 parameters for the five atoms in special positions which can only move along the fixed two-fold axes in the unit cell. The functional forms of the partial derivatives of the  $F(hkl)$  are obtained by differentiating the expression for  $F(hkl)$  given on p. 28. These partials are functions of all the parameters and must be numerically evaluated by substitution of the approximate parameters which are to be refined. The  $F_{\text{obs}}$  are on an absolute scale, i.e. they contain the scale factors which had previously been determined. They also must be assigned the signs of the corresponding  $F_{\text{calc}}$ . The  $F_{\text{calc}}$  are calculated from the trial parameters. One such observational equation can be used for each combination of (hkl) for which an intensity was measured and for which the calculated F is large enough so that there is no question about the correctness of its sign. In the successive three least squares procedures carried out on this structure, 410, 416, and 420 equations were used, respectively. Each equation was multiplied

by the square root of its weight, described below. The 400 odd weighted equations were then reduced to 23 normal equations by standard procedures, described, for instance, in Whittaker and Robinson<sup>(12)</sup>. The solution of the 23 normal equations gives values for the parameter shifts  $\Delta x_i$  by which the corresponding parameters  $x_i$  should be corrected. With these new  $x_i$  the procedure is repeated. A new set of  $F(hk\ell)$  and their derivatives are calculated, and another least squares procedure is carried out, resulting in new  $\Delta x_i$  for further corrections on the  $x_i$ . The procedure is repeated until the parameter shifts  $\Delta x_i$  have become negligibly small.

#### Methods of Calculation

All calculations leading to the observational equations were carried out on punched cards by means of an IBM electronic multiplier, model 604. The procedures making use of this machine included the calculation of the  $F(hk\ell)$  (one step of which was carried out on the IBM Tabulator, model 402), their derivatives, and the temperature factors for each equation. The IBM machines were also used to multiply the observational equations by the square roots of their weights, and to reduce the weighted equations to 23 normal equations. The latter step in particular would have been a staggering job if carried out on a desk calculator. The solution of the normal equations, however, was carried out on a desk calculator by means of an iteration procedure described in Whittaker and Robinson. At the end of each procedure the probable errors

of all the parameter shifts were calculated by an approximation formula. The approximate formula is obtained by evaluating the quantities in the exact formula, given in the above reference, on the assumption that all the non-diagonal elements in the normal equations are zero. In actual practice they are reasonably small compared to the diagonal elements.

### The Weighting of the Observational Equations

The method of weighting used in this investigation is somewhat of an elaboration on the method first proposed by Hughes. Theoretically, the weight should be proportional to the inverse square of the absolute error in  $F_{\text{obs}}$ . Hughes proposed that the percentage error in the observed intensities stays about constant over a large range of intensities and increases linearly with decreasing intensity below an intensity which is four times the value of the minimum observable intensity for the particular film. In other words, for intensities greater than four times the minimum observable one, the percent error is constant, below that the absolute error is constant. This can be expressed as

$$\begin{aligned} \sqrt{w_{hke}} &= \frac{1}{rF} & i > 4i_{\text{min}} \\ &= \frac{i}{4i_{\text{min}} rF} & i \leq 4i_{\text{min}} \end{aligned}$$

Here  $i$  is the uncorrected intensity of the spot as it appears on the film. The quantity  $r$  represents the percentage error in  $F$ . Although  $r$  is constant for a given film in the Hughes method, it is best to estimate it since it might change some-

what from film to film, depending on the quality of the latter. The value of  $i_{\min}$  must also be determined separately for each film.  $F$  in this formula should be on an absolute scale, or at least on the same scale for all films.

This method of weighting was extended in two ways. In the first place it was found that in some slightly overexposed films the most intense spots could not be measured with the same accuracy as the spots in the middle region of intensity. In these cases an upper value for the intensity was decided upon, above which the percentage error was increased linearly with increasing intensity. The slope of the increase was decided by actually estimating the errors of some of the more intense spots. This could be done by fixing an upper and lower limit to the intensity value of a given spot and by checking the reproducibility of measurements taken at different times.

The second extension of the Hughes method of weighting consisted of making the percentage error  $r$  a function of the Bragg angle  $\theta$ . It becomes quite difficult to obtain reproducible intensity measurements when the spot to be measured and the comparison spots are of different shape. The comparison spots on the intensity strip are all of the same shape. The spots on the Weissenberg photographs change their shapes as a function of  $\theta$ . For instance, the upper layer Weissenberg photographs taken around the needle axis  $c_0$  showed the familiar phenomenon of compaction of the spots

on one half of the film and extension on the other half. The degree of compaction or extension varies with  $\theta$ . This effect is discussed in some detail in Buerger<sup>(16)</sup>. Another cause for the change of the shape of spots with changing Bragg angle is the splitting of the  $\alpha$  doublet into  $\alpha_1$  and  $\alpha_2$ , a phenomenon which starts in the region of  $\sin \theta \cong 0.78$ . In this region the spots begin to broaden. At higher values of  $\sin \theta$ , when the splitting is complete, each component of the doublet has to be measured separately and is sharper than the comparison spots.

The function  $r(\theta)$  was determined empirically for each film. The percentage error in some spots at varying values of  $\theta$  was estimated and plotted against  $\theta$ . The percentage error of all the spots was then taken from these curves. The curves are not reproduced here. They are quite subjective and have meaning only for the experimenter who made them and did the intensity measurements. It is usually found that the final results in this kind of work are relatively insensitive to the exact method of weighting the data. Nevertheless, all the weights will be listed together with the  $F_{\text{obs}}$  and the final set of  $F_{\text{calc}}$  for the sake of completeness, so that all the calculations could, in principle, be reproduced or continued further. This listing is given in Table III, page 50. The weights are given in form of their square roots, which is the form in which they are actually used in the calculation. Their absolute values have no significance, having been adjusted to a numerical range which was found convenient for the punched card calculations.

### Resulting Parameters

The parameters, in terms of unit cell fractions, at the various stages of refinement are given in Table I. Column 1 contains the model based on the half-cell projection. Columns 2, 3, and 4, are the parameter shifts obtained in three successive least squares procedures. Column 5 corresponds to the final model, obtained by algebraic addition of columns 1, 2, 3, and 4. Column 6 contains the probable errors which have been adopted for the parameters.

It has been mentioned previously that the probable errors are obtained in the course of the least squares procedure by an approximation formula. They have meaning only, however, when the successive procedures have converged to a point where the indicated parameter shifts are less than the "proper" probable errors calculated by the formula. Column 5 shows that the last set of parameter shifts had not all converged to such small values. Three of the y-parameter shifts are still as large as about 0.02 Å. (Their values in Ångstroms are obtained by multiplying them by the appropriate unit cell axis length.) Time limitations made it impossible to carry out another least squares procedure. However, an extrapolation of the root mean square values of the parameter shifts in the three procedures indicated that the rms value of the shifts for another procedure would be only 0.004 Å. In principle, therefore, 0.004 should be multiplied by 0.6745 and the result added vectorially to the

Table I

Parameters, in unit cell fractions, at various stages of their refinement and probable errors, in the same units, of the final set of parameters.

	1	2	3	4	5	6
y(O <sub>1</sub> )	0.192	0.00059	0.00075	0.00107	0.1944	0.00040
y(O <sub>2</sub> )	.177	.00049	-.00023	-.00002	.1772	.00034
y(O <sub>3</sub> )	.090	-.00181	-.00107	-.00082	.0863	.00035
y(O <sub>4</sub> )	-.129	.00057	.00007	.00008	-.1283	.00034
y(N <sub>1</sub> )	.120	-.00156	-.00049	-.00014	.1178	.00038
y(N <sub>2</sub> )	-.097	.00073	-.00037	-.00058	-.0972	.00051
y(C <sub>1</sub> )	.127	.00013	.00148	-.00106	.1276	.00056
y(C <sub>2</sub> )	.086	.00019	-.00125	-.00009	.0849	.00042
y(C <sub>3</sub> )	.012	.00146	.00032	-.00059	.0132	.00047
y(C <sub>4</sub> )	-.021	-.00083	-.00139	.00020	-.0230	.00058
x(K <sup>+</sup> )	.133	-.00038	-.00001	.00013	.1327	.00025
x(O <sub>2</sub> )	.195	-.00221	.00073	.00020	.1937	.00041
x(O <sub>3</sub> )	.231	-.00374	-.00232	-.00065	.2243	.00045
x(O <sub>4</sub> )	.069	.00242	-.00004	-.00043	.0710	.00043
x(N <sub>1</sub> )	.173	.00089	.00172	.00010	.1757	.00047
x(C <sub>2</sub> )	.082	.00161	.00070	.00062	.0849	.00054
x(C <sub>3</sub> )	.081	.00291	.00105	-.00040	.0846	.00056
z(O <sub>2</sub> )	.176	-.00282	.00006	-.00012	.1731	.00097
z(O <sub>3</sub> )	.010	-.01198	.00000	-.00047	-.0025	.00109
z(O <sub>4</sub> )	.196	-.01238	-.00462	-.00044	.1786	.00085
z(N <sub>1</sub> )	.114	-.00045	-.00354	-.00032	.1097	.00137
z(C <sub>2</sub> )	.185	.00286	-.00182	.00077	.1868	.00120
z(C <sub>3</sub> )	.186	.00162	-.00396	-.00038	.1833	.00129

Table II

Parameters and their Probable Errors in Angstroms

Atom	x	y	z
O <sub>1</sub>	0	3.725 ± 0.008	1.789 ± 0.000
C <sub>1</sub>	0	2.443 ± .011	1.789 ± .000
C <sub>2</sub>	1.132 ± 0.007	1.626 ± .008	1.337 ± .009
N <sub>1</sub>	2.342 ± .006	2.256 ± .007	0.784 ± .010
O <sub>2</sub>	2.582 ± .005	3.396 ± .007	1.239 ± .007
O <sub>3</sub>	2.990 ± .006	1.654 ± .007	-0.018 ± .008
C <sub>3</sub>	1.127 ± .007	0.253 ± .009	1.311 ± .009
C <sub>4</sub>	0	-0.440 ± .011	1.789 ± .000
N <sub>2</sub>	0	-1.863 ± .010	1.789 ± .000
O <sub>4</sub>	0.945 ± .006	-2.457 ± .007	1.277 ± .006
K <sup>+</sup>	1.769 ± .003	4.790 ± .000	3.577 ± .000

"proper" probable errors. In order to be on the conservative side, the factor 0.6745 was omitted. In other words, the probable errors in column 6, Table I, are equal to the square root of the sum of the squares of the proper probable errors plus  $(0.004)^2$ . Table II gives all the parameters of the atoms in the asymmetric unit, including the ones fixed by space group requirements, in Ångstroms. It also gives the adopted probable errors in Ångstroms.

Finally, Table III contains the observed and calculated structure factors, and, for the record, the square roots of the weights which were used. All the structure factors should be multiplied by 8 in order to be on a truly absolute scale. The factor 8 derives from the eight molecules per unit cell, but was dropped in all the calculations for the sake of convenience. It should be pointed out that the  $F_{\text{calc}}$  in Table III are based on the next to last set of parameters, which can be obtained by adding columns 1, 2, and 3 of Table I. It was not considered worth while to calculate a new set of structure factors from the final parameters, since this would not have added to the accuracy of the structure, but would merely have made the agreement in Table III look a little better. The reliability factor corresponding to Table III is 13.9%. It is a measure of the discrepancy between calculated and observed structure factors and is defined by

$$R = \sum \frac{||F_{\text{obs}}| - |F_{\text{calc}}||}{|F_{\text{obs}}|}$$

The summation does not include those  $F_{\text{calc}}$  for which the corresponding  $F_{\text{obs}}$  were too weak to be measured.

Table III

Observed and Calculated Structure Factors and Weights

Some indices correspond to reflections outside the limits of Cu K $\alpha$  radiation. The intensities of such spots were measured from Cu K $\beta$  reflections. The abbreviation n.o. means not observable due to camera limitations. All structure factors should be multiplied by eight if they are to be on a truly absolute scale.

Index	F <sub>obs</sub>	F <sub>calc</sub>	$\sqrt{w}$	Index	F <sub>obs</sub>	F <sub>calc</sub>	$\sqrt{w}$
<u>0k0</u>				<u>2k0</u>			
2	1.6	- 2.4	1.09	8	10.8	9.7	0.10
4	16.6	-20.4	0.03	10	3.9	1.3	0.50
6	12.2	-15.1	0.08	12	9.3	-10.0	0.21
8	19.1	18.3	0.03	14	5.1	4.5	0.39
10	10.9	8.5	0.11	16	1.6	1.5	0.48
12	11.6	11.9	0.15	18	4.0	- 3.5	0.49
14	11.9	-11.7	0.14	20	< 1.1	0.3	0.00
16	11.7	10.2	0.17	22	< 1.0	- 0.6	0.00
18	9.9	-11.1	0.20	24	1.3	- 1.6	1.00
20	2.0	- 2.5	0.66	<u>4k0</u>			
22	1.3	- 0.4	0.30	0	2.0	2.1	1.16
24	5.4	6.2	0.37	2	10.7	11.9	0.17
26	4.0	- 4.4	0.25	4	16.6	-17.6	0.04
<u>2k0</u>				6	9.2	7.2	0.14
0	8.7	8.3	0.19	8	16.3	-17.5	0.06
2	8.8	8.5	0.13	10	13.4	15.0	0.08
4	3.6	4.1	0.55	12	6.7	- 4.8	0.29
6	7.2	7.2	0.27	14	5.2	3.8	0.38

Table III (Cont.)

Index	F <sub>obs</sub>	F <sub>calc</sub>	$\sqrt{w}$	Index	F <sub>obs</sub>	F <sub>calc</sub>	$\sqrt{w}$
<u>4k0</u>				<u>8k0</u>			
16	8.0	- 7.7	0.25	6	10.6	-12.4	0.15
18	2.5	0.9	0.71	8	4.2	2.5	0.46
20	3.8	- 3.2	0.29	10	5.4	- 4.2	0.37
22	4.7	4.9	0.45	12	6.4	6.2	0.31
24	4.1	- 3.4	0.24	14	4.7	- 3.3	0.42
<u>6k0</u>				16	< 0.9	- 0.5	0.00
0	5.9	4.2	0.38	18	6.0	- 6.8	0.16
2	15.2	-14.4	0.12	20	6.5	7.1	0.30
4	2.0	2.1	1.00	22	3.6	- 3.2	0.24
6	5.4	4.4	0.37	<u>10k0</u>			
8	<1.0	- 2.0	0.00	0	10.2	10.8	0.21
10	< 0.9	- 0.8	0.00	2	3.8	3.3	0.58
12	5.4	- 3.9	0.37	4	4.9	- 3.7	0.40
14	9.2	- 9.9	0.21	6	6.7	6.8	0.29
16	4.9	4.2	0.40	8	7.2	- 5.6	0.27
18	< 1.4	2.2	0.00	10	7.8	7.4	0.25
20	2.0	1.4	0.37	12	< 1.3	0.7	0.00
22	2.9	- 3.2	0.67	14	< 1.1	- 0.7	0.00
24	n.o.	- 1.7	0.00	16	1.6	- 1.4	0.40
<u>8k0</u>				18	< 1.0	- 0.4	0.00
0	1.7	0.3	0.79	20	2.9	- 2.9	0.18
2	6.0	- 6.0	0.32	22	1.8	2.3	0.20
4	13.0	15.3	0.08				

Table III (Cont.)

Index	F <sub>obs</sub>	F <sub>calc</sub>	$\sqrt{w}$	Index	F <sub>obs</sub>	F <sub>calc</sub>	$\sqrt{w}$
<u>12k0</u>				<u>16k0</u>			
0	7.6	7.3	0.29	8	n.o.	3.0	0.00
2	8.9	9.0	0.25	10	n.o.	- 2.4	0.00
4	7.5	- 7.7	0.26	12	n.o.	- 1.2	0.00
6	4.1	4.0	0.48	<u>18k0</u>			
8	2.0	1.7	0.62	0	2.0	- 1.6	0.19
10	7.8	8.0	0.25	2	n.o.	2.1	0.00
12	5.9	- 5.6	0.17	4	3.4	- 3.7	0.29
14	4.1	3.7	0.35	<u>1k1</u>			
16	1.5	- 1.4	0.84	2	6.6	- 5.4	0.34
18	n.o.	0.2	0.00	4	6.8	7.2	0.29
20	2.9	- 3.4	0.33	6	10.2	-10.9	0.20
<u>14k0</u>				8	2.8	1.2	0.70
0	9.6	9.8	0.21	10	7.9	7.6	0.25
2	< 1.2	- 0.5	0.00	12	4.7	- 4.4	0.42
4	2.6	1.1	0.55	14	< 1.7	- 0.9	0.00
6	3.3	- 3.3	0.30	16	2.5	- 1.9	0.60
8	3.3	3.4	0.35	18	2.4	- 2.4	0.57
10	< 1.4	- 0.3	0.00	20	< 1.7	0.0	0.00
12	2.0	2.5	1.00	22	< 1.5	- 0.7	0.00
<u>16k0</u>				<u>2k1</u>			
0	5.1	5.7	0.43	1	5.9	6.7	0.34
2	4.8	- 5.2	0.47	3	20.0	-24.0	0.03
4	1.6	0.2	0.84	5	11.9	12.4	0.09
6	n.o.	0.6	0.00				

Table III (Cont.)

Index	F <sub>Obs</sub>	F <sub>calc</sub>	$\sqrt{w}$	Index	F <sub>Obs</sub>	F <sub>calc</sub>	$\sqrt{w}$
<u>2k1</u>				<u>4k1</u>			
7	10.2	-10.6	0.20	5	10.4	-10.4	0.19
9	14.2	15.0	0.11	7	3.8	- 3.6	0.53
11	9.8	-10.0	0.20	9	4.1	- 3.3	0.49
13	4.2	2.0	0.48	11	4.4	3.7	0.43
15	7.2	- 6.9	0.28	13	1.9	- 1.0	0.56
17	5.4	5.0	0.37	15	3.8	- 2.9	0.52
19	5.4	- 5.7	0.22	17	< 2.0	- 0.4	0.00
21	5.0	4.2	0.23	19	2.6	2.1	0.42
23	3.8	- 3.1	0.28	21	3.4	- 3.1	0.35
				23	< 1.6	- 0.6	0.00
<u>3k1</u>				<u>5k1</u>			
2	12.4	14.1	0.13	2	10.9	-12.3	0.21
4	3.1	3.0	0.64	4	17.8	20.3	0.09
6	4.6	- 4.7	0.43	6	5.6	5.1	0.35
8	2.4	1.7	0.83	8	4.2	- 3.8	0.48
10	< 1.4	0.0	0.00	10	< 1.6	0.5	0.00
12	5.2	5.5	0.38	12	< 1.6	0.5	0.00
14	4.2	3.9	0.48	14	11.8	12.3	0.17
16	4.0	- 4.1	0.50	16	5.1	5.0	0.39
18	2.3	1.8	0.52	18	4.9	- 4.4	0.24
20	1.3	1.4	0.22	20	1.8	1.3	0.35
22	1.1	- 1.4	0.19	22	3.0	2.7	0.59
<u>4k1</u>							
1	10.4	12.1	0.19				
3	11.2	13.0	0.18				

Table III (Cont.)

Index	F <sub>obs</sub>	F <sub>calc</sub>	$\sqrt{w}$	Index	F <sub>obs</sub>	F <sub>calc</sub>	$\sqrt{w}$
<u>6k1</u>				<u>8k1</u>			
1	13.9	-17.0	0.14	1	5.9	5.6	0.34
3	4.3	4.0	0.46	3	1.9	1.6	0.68
5	9.9	-10.1	0.20	5	7.8	7.4	0.26
7	8.6	9.9	0.23	7	3.0	- 3.0	0.68
9	2.5	- 1.4	0.76	9	3.1	- 3.5	0.64
11	8.1	7.8	0.24	11	5.5	- 4.6	0.36
13	8.9	-10.1	0.00	13	6.3	6.7	0.32
15	5.0	4.2	0.38	15	3.0	3.0	0.66
17	5.1	- 4.3	0.27	17	2.4	2.3	0.40
19	4.3	4.3	0.27	19	3.2	- 3.2	0.37
21	2.8	- 1.7	0.41	21	n.o.	- 0.1	0.00
<u>7k1</u>				<u>9k1</u>			
2	1.1	- 1.9	1.33	2	2.2	- 1.6	0.98
4	7.4	6.6	0.27	4	5.6	5.0	0.35
6	7.5	7.7	0.27	6	< 1.8	0.3	0.00
8	< 1.6	0.0	0.00	8	2.1	- 1.1	0.52
10	6.1	- 6.4	0.33	10	1.5	- 0.3	0.36
12	4.8	5.4	0.42	12	2.7	2.2	0.64
14	10.3	11.3	0.19	14	3.8	4.2	0.37
16	< 1.8	0.1	0.00	16	1.6	- 2.0	0.27
18	1.6	- 1.2	0.28	18	1.7	- 1.7	0.27
20	2.0	1.2	0.34	20	2.0	1.7	1.00
22	1.2	1.3	0.90				

Table III (Cont.)

Index	F <sub>obs</sub>	F <sub>calc</sub>	$\sqrt{w}$	Index	F <sub>obs</sub>	F <sub>calc</sub>	$\sqrt{w}$
<u>10.k.1</u>				<u>12.k.1</u>			
1	6.4	5.5	0.31	7	2.1	1.3	0.47
3	7.7	- 8.4	0.26	9	4.9	- 5.4	0.24
5	5.0	4.3	0.40	11	1.5	0.6	0.26
7	4.6	- 3.3	0.43	13	2.0	- 0.8	0.37
9	7.2	7.3	0.28	15	4.7	5.0	0.30
11	2.6	- 2.4	0.61	17	n.o.	- 2.1	0.00
13	4.5	4.2	0.26	<u>13.k.1</u>			
15	5.9	- 5.9	0.20	2	< 2.0	2.3	0.00
17	4.3	3.0	0.26	4	1.9	- 1.5	0.26
19	1.5	- 0.3	0.85	6	1.4	- 1.9	0.16
<u>11.k.1</u>				8	1.8	1.7	0.23
2	5.9	- 6.0	0.38	10	< 1.9	0.4	0.00
4	3.3	2.9	0.60	12	< 1.8	0.6	0.00
6	1.5	- 0.8	0.35	14	< 1.6	- 0.6	0.00
8	< 1.9	0.2	0.00	<u>14.k.1</u>			
10	1.5	1.4	0.37	1	4.6	- 4.2	0.19
12	2.3	- 2.4	0.36	3	1.2	0.1	0.15
14	2.0	1.0	0.38	5	4.9	- 5.0	0.18
16	2.6	- 1.1	0.45	7	5.7	5.4	0.15
18	3.4	- 3.3	0.59	9	3.1	- 1.9	0.28
<u>12.k.1</u>				11	2.7	2.3	0.35
1	4.8	- 4.3	0.40	13	3.2	- 3.5	0.42
3	4.9	4.4	0.40				
5	< 1.4	0.6	0.00				

Table III (Cont.)

Index	F <sub>obs</sub>	F <sub>calc</sub>	$\sqrt{w}$	Index	F <sub>obs</sub>	F <sub>calc</sub>	$\sqrt{w}$
<u>15.k.1</u>				<u>2k3</u>			
2	<1.8	1.0	0.00	3	10.9	-11.7	0.12
4	4.2	3.7	0.20	5	12.7	12.1	0.10
6	2.4	- 2.4	0.31	7	3.9	- 2.1	0.35
8	<1.5	- 0.6	0.00	9	5.0	3.9	0.30
10	3.0	3.3	0.45	11	7.6	- 7.0	0.26
<u>16.k.1</u>				13	12.0	13.3	0.12
1	3.8	3.4	0.28	15	4.2	- 4.2	0.29
3	1.7	- 0.6	0.35	17	5.8	5.0	0.19
5	2.2	1.5	0.61	19	2.8	- 1.7	0.24
7	3.8	- 4.4	0.35	21	3.9	4.1	0.32
<u>1k3</u>				23	n.o.	- 1.9	0.00
2	1.1	- 1.3	1.42	<u>3k3</u>			
4	6.2	- 6.6	0.21	2	7.1	5.4	0.27
6	5.1	5.2	0.26	4	7.8	- 5.4	0.17
8	<0.9	0.4	0.00	6	5.0	- 3.5	0.28
10	3.9	- 3.7	0.46	8	1.3	- 1.5	0.55
12	1.3	- 0.8	0.00	10	3.2	2.7	0.61
14	2.9	- 2.2	0.45	12	<1.1	- 0.0	0.00
16	2.3	2.2	0.43	14	7.7	- 7.0	0.16
18	1.3	1.1	0.20	16	<0.9	- 0.5	0.00
20	1.7	- 1.4	0.36	18	3.1	2.4	0.31
22	<0.9	0.3	0.00	20	<0.9	0.4	0.00
<u>2k3</u>				22	1.3	- 0.8	0.55
1	14.4	14.0	0.09				

Table III (Cont.)

Index	F <sub>obs</sub>	F <sub>calc</sub>	$\sqrt{w}$	Index	F <sub>obs</sub>	F <sub>calc</sub>	$\sqrt{w}$
<u>4k3</u>				<u>6k3</u>			
1	10.5	-11.2	0.13	1	8.3	- 7.6	0.18
3	7.0	4.9	0.20	3	1.8	0.9	0.77
5	12.8	12.8	0.11	5	11.5	-10.9	0.17
7	<1.0	- 1.2	0.00	7	13.9	14.2	0.14
9	7.1	- 6.9	0.32	9	6.7	- 6.2	0.24
11	1.1	- 0.9	0.33	11	5.7	5.0	0.23
13	3.9	3.4	0.34	13	3.9	- 3.5	0.31
15	9.6	10.9	0.12	15	1.5	0.5	0.28
17	1.5	- 0.9	0.23	17	4.6	- 4.9	0.20
19	2.2	- 2.8	0.45	19	5.0	5.6	0.24
21	2.2	1.5	0.47	21	2.7	- 2.5	0.51
<u>5k3</u>				<u>7k3</u>			
2	2.0	- 1.6	1.00	2	0.9	0.2	0.73
4	8.2	- 8.5	0.18	4	7.0	- 5.8	0.28
6	1.3	2.3	0.58	6	<1.1	- 0.8	0.00
8	1.2	1.6	0.51	8	1.7	0.6	0.47
10	2.3	- 2.4	0.66	10	<1.1	0.5	0.00
12	3.5	- 2.6	0.37	12	2.7	- 2.2	0.45
14	5.3	- 4.7	0.23	14	5.3	- 5.6	0.21
16	< 0.9	0.4	0.00	16	< 1.2	0.1	0.00
18	< 0.9	0.7	0.00	18	1.3	1.1	0.25
20	2.1	- 1.8	0.47	20	1.3	- 0.9	0.59
22	< 0.9	- 0.2	0.00				

Table III (Cont.)

Index	F <sub>obs</sub>	F <sub>calc</sub>	$\sqrt{w}$	Index	F <sub>obs</sub>	F <sub>calc</sub>	$\sqrt{w}$
<u>8k3</u>				<u>10.k.3</u>			
1	4.6	4.3	0.39	5	1.7	1.0	0.33
3	<1.1	1.2	0.00	7	4.3	- 4.4	0.28
5	1.6	0.9	0.45	9	7.9	9.7	0.14
7	7.7	- 7.7	0.18	11	4.0	- 3.3	0.24
9	1.8	1.5	0.37	13	1.3	- 2.5	0.22
11	1.8	- 1.8	0.33	15	6.5	- 6.7	0.19
13	1.5	- 0.8	0.24	17	1.5	2.4	0.58
15	3.9	- 2.9	0.23	<u>11.k.3</u>			
17	<1.1	0.4	0.00	2	1.2	- 0.8	0.24
19	2.2	- 2.6	0.63	4	2.0	- 2.8	0.36
<u>9k3</u>				6	2.2	2.2	0.37
2	4.3	4.1	0.46	8	1.2	0.6	0.19
4	3.9	- 3.2	0.35	10	1.8	- 2.0	0.28
6	3.1	2.6	0.42	12	1.2	- 1.0	0.25
8	<1.2	- 0.8	0.00	14	1.1	- 1.0	0.24
10	1.6	1.7	0.28	16	1.8	1.7	0.76
12	<1.2	- 0.2	0.00	<u>12.k.3</u>			
14	4.8	- 4.8	0.19	1	1.8	3.0	0.28
16	<1.2	- 0.2	0.00	3	5.3	6.6	0.20
18	2.3	2.2	0.60	5	3.9	- 4.6	0.25
<u>10.k.3</u>				7	2.2	1.4	0.36
1	2.3	2.3	0.48	9	3.8	- 3.6	0.25
3	10.3	- 9.5	0.12	11	2.7	2.4	0.42

Table III (Cont.)

Index	F <sub>obs</sub>	F <sub>calc</sub>	$\sqrt{w}$	Index	F <sub>obs</sub>	F <sub>calc</sub>	$\sqrt{w}$
<u>12.k.3</u>				<u>16.k.3</u>			
13	1.2	- 0.2	0.35	1	n.o.	2.7	0.00
15	1.1	1.2	0.70	3	n.o.	- 1.3	0.00
<u>13.k.3</u>				<u>1k5</u>			
2	0.9	0.8	0.64	2	0.7	- 0.8	0.53
4	1.7	- 1.3	0.28	4	6.3	4.8	0.16
6	<1.3	0.6	0.00	6	3.4	2.6	0.36
8	<1.3	- 0.6	0.00	8	<1.1	- 0.2	0.00
10	<1.1	- 0.2	0.00	10	1.6	- 1.8	0.55
12	n.o.	- 0.4	0.00	12	3.7	3.0	0.28
14	n.o.	- 1.7	0.00	14	7.1	6.2	0.20
<u>14.k.3.</u>				16	<1.1	- 0.3	0.00
1	3.8	- 4.6	0.28	18	1.0	- 1.0	0.27
3	4.0	3.7	0.27	20	1.1	1.1	1.01
5	1.5	- 1.2	0.26	<u>2k5</u>			
7	1.8	1.8	0.46	1	7.9	6.8	0.12
9	1.1	- 0.6	0.36	3	8.1	- 6.3	0.13
11	3.3	3.9	0.44	5	2.0	1.7	0.58
<u>15.k.3</u>				7	9.9	-10.3	0.14
2	2.0	1.0	0.99	9	10.2	10.5	0.14
4	1.6	- 1.9	0.52	11	3.9	- 2.2	0.30
6	1.5	- 0.7	0.60	13	1.0	- 1.2	0.29
8	0.6	- 0.3	0.63	15	9.1	- 8.5	0.14

Table III (Cont.)

Index	F <sub>obs</sub>	F <sub>calc</sub>	$\sqrt{w}$	Index	F <sub>obs</sub>	F <sub>calc</sub>	$\sqrt{w}$
<u>2k5</u>				<u>5k5</u>			
17	3.2	2.8	0.32	2	2.5	2.9	0.78
19	2.5	- 2.0	0.65	4	< 1.3	- 0.0	0.00
				6	1.1	- 1.5	0.00
<u>3k5</u>				8	< 1.2	1.1	0.00
2	5.5	- 4.9	0.33	10	< 1.2	- 0.3	0.00
4	6.4	6.4	0.19	12	2.3	1.5	0.59
6	2.0	0.3	0.62	14	1.9	1.2	0.56
8	< 0.8	- 0.8	0.00	16	3.0	- 2.6	0.34
10	1.4	1.3	0.40	18	0.8	0.2	0.53
12	< 1.3	- 0.6	0.00				
14	5.3	4.1	0.26	<u>6k5</u>			
16	< 1.4	0.8	0.00	1	7.1	- 7.3	0.20
18	3.2	- 2.7	0.46	3	4.5	4.5	0.32
20	1.2	0.7	1.50	5	6.4	- 6.2	0.23
				7	4.7	3.4	0.27
<u>4k5</u>				9	2.0	- 0.4	0.49
1	1.1	1.7	0.52	11	5.8	6.2	0.24
3	1.1	0.2	0.50	13	6.0	- 6.8	0.20
5	3.7	- 4.4	0.41	15	3.4	2.2	0.30
7	3.1	2.8	0.47	17	3.4	- 2.6	0.48
9	2.7	- 2.3	0.50				
11	2.2	- 1.6	0.45	<u>7k5</u>			
13	2.8	- 1.6	0.51	2	1.6	- 0.7	1.02
15	< 1.0	- 0.9	0.00	4	3.3	3.2	0.39
17	1.5	- 0.8	0.38	6	2.3	- 2.7	0.46
19	< 0.7	- 0.6	0.00	8	< 1.3	- 0.1	0.00

Table III (Cont.)

Index	F <sub>obs</sub>	F <sub>calc</sub>	$\sqrt{w}$	Index	F <sub>obs</sub>	F <sub>calc</sub>	$\sqrt{w}$
<u>7k5</u>				<u>9k5</u>			
10	2.8	2.9	0.51	14	3.0	2.6	0.55
12	<1.2	- 0.8	0.00	16	n.o.	0.3	0.00
14	<1.2	0.5	0.00	<u>10.k.5</u>			
16	1.1	- 0.5	0.45	1	1.4	1.3	0.48
18	1.2	- 1.2	1.43	3	5.9	- 7.1	0.23
<u>8k5</u>				5	5.8	5.8	0.22
1	5.5	5.1	0.20	7	< 1.4	0.9	0.00
3	3.8	3.3	0.28	9	2.9	2.6	0.35
5	3.9	3.9	0.28	11	3.7	- 4.4	0.29
7	3.6	- 3.2	0.36	13	4.6	4.8	0.38
9	1.1	- 1.5	0.32	15	n.o.	- 0.5	0.00
11	1.2	- 0.9	0.35	<u>11.k.5</u>			
13	5.0	5.2	0.20	2	1.6	1.3	0.75
15	1.5	1.7	0.66	4	2.2	1.9	0.47
17	2.0	2.2	0.90	6	1.0	0.7	0.17
<u>9k5</u>				8	<1.4	0.3	0.00
2	1.0	0.0	0.26	10	<1.4	- 0.4	0.00
4	2.5	2.7	0.51	12	2.0	2.1	0.86
6	<1.4	- 0.2	0.00	<u>12.k.5</u>			
8	<1.4	0.2	0.00	1	1.7	- 2.3	0.33
10	<1.4	0.6	0.00	3	3.7	3.7	0.28
12	0.9	0.5	0.20	5	1.3	- 0.3	0.34

Table III (Cont.)

Index	F <sub>obs</sub>	F <sub>calc</sub>	$\sqrt{w}$	Index	F <sub>obs</sub>	F <sub>calc</sub>	$\sqrt{w}$
<u>12.k.5</u>				<u>40ℓ</u>			
7	<1.3	- 0.5	0.00	2	14.9	-13.9	0.12
9	2.5	- 3.1	0.66	4	9.1	6.6	0.19
11	1.6	1.7	1.13	6	10.3	- 9.0	0.18
				8	2.7	2.4	0.47
<u>13.k.5</u>				<u>60ℓ</u>			
2	1.3	- 1.7	1.46	2	3.4	- 3.7	0.51
4	2.7	3.6	0.64	4	3.6	3.5	0.49
6	<1.3	1.0	0.00	6	9.4	- 9.8	0.19
8	<1.3	- 0.8	0.00	8	7.6	6.7	0.23
<u>14.k.5</u>				<u>80ℓ</u>			
1	2.1	- 2.5	0.83	2	9.0	8.4	0.17
3	<0.5	- 0.2	0.00	4	15.4	17.3	0.10
5	n.o.	- 4.3	0.00	6	3.2	- 3.7	0.49
				8	5.3	7.5	0.00
<u>00ℓ</u>				<u>10.0.ℓ</u>			
2	15.4	-14.4	0.11	2	13.3	-13.2	0.12
4	17.2	16.5	0.10	4	2.5	1.5	0.52
6	10.4	12.1	0.17	6	3.2	- 2.3	0.32
8	5.1	3.4	0.18				
<u>20ℓ</u>				<u>12.0.ℓ</u>			
2	26.1	-34.2	0.04	2	12.7	-13.4	0.12
4	9.3	5.7	0.19	4	2.7	- 1.9	0.53
6	7.7	7.1	0.23	6	4.5	- 4.1	0.34
8	1.2	- 0.9	0.13				

Table III (Cont.)

Index	F <sub>obs</sub>	F <sub>calc</sub>	$\sqrt{w}$	Index	F <sub>obs</sub>	F <sub>calc</sub>	$\sqrt{w}$
<u>14.0.l</u>				<u>h26</u>			
2	2.8	- 2.5	0.38	0	3.2	- 3.7	0.55
4	8.2	7.5	0.19	2	1.1	1.6	0.73
<u>16.0.l</u>				4	2.9	4.3	0.60
2	2.0	- 2.1	0.70	6	5.3	- 5.4	0.34
<u>h22</u>				8	3.5	- 3.2	0.51
0	16.1	-11.7	0.05	10	1.5	1.4	0.51
2	12.3	- 9.8	0.14	12	3.4	3.9	0.52
4	18.7	17.9	0.04	<u>h27</u>			
6	0.6	0.5	0.56	1	<0.8	1.3	0.00
8	7.2	- 7.3	0.25	3	0.9	0.5	0.62
10	2.6	2.4	0.68	5	1.6	0.5	0.98
12	1.0	1.0	0.64	7	1.2	0.8	0.61
14	2.8	- 3.2	0.18	9	1.4	- 1.8	1.27
16	1.7	- 1.9	1.05	11	n.o.	- 0.2	0.00
<u>h24</u>				<u>h28</u>			
0	5.5	- 5.3	0.32	0	3.5	- 3.4	0.29
2	2.3	- 2.8	0.78	2	0.9	- 1.8	0.32
4	11.1	10.5	0.16	4	4.5	5.0	0.32
6	1.8	- 2.5	0.99	6	1.6	1.3	1.10
8	5.4	- 5.2	0.33	8	n.o.	- 1.8	0.00
10	3.3	3.0	0.54	<u>h29</u>			
12	2.6	3.0	0.60	1	n.o.	0.1	0.00
14	1.7	- 1.3	1.04	3	n.o.	- 0.9	0.00

## DESCRIPTION AND DISCUSSION OF THE STRUCTURE

### Internal Configuration of the Picrate Ion

Figure 6 is a projection of the picrate ion onto the average plane through its benzene ring, which is not quite planar, although the deviation from planarity is within experimental uncertainty. The circles represent carbon, nitrogen, and oxygen atoms in order of increasing diameters. The two hydrogen atoms of the picrate ion are not shown, because their positions were not determined experimentally. Each circle is labeled with the chemical symbol for the atom it represents, plus a subscript to differentiate between crystallographically different atoms of the same species. In addition, each circle contains a number which is equal to its distance in Angstroms above (negative) or below (positive) the plane of the paper. The thickness of the circles is calculated to give an impression of depth, the thickest ones being furthest above the plane of the paper, the thinnest ones furthest below. The sticks, representing bonds, are also drawn to give an impression of depth.

A two-fold axis passes through the centers of atoms  $O_1$ ,  $C_1$ ,  $C_4$ , and  $N_2$ . This axis generates the primed atoms in the lower half of the molecule in Figure 6 from the corresponding unprimed ones in the upper half, the latter constituting the asymmetric unit of the whole structure excepting the potassium ion. The bond distances and angles in the lower half

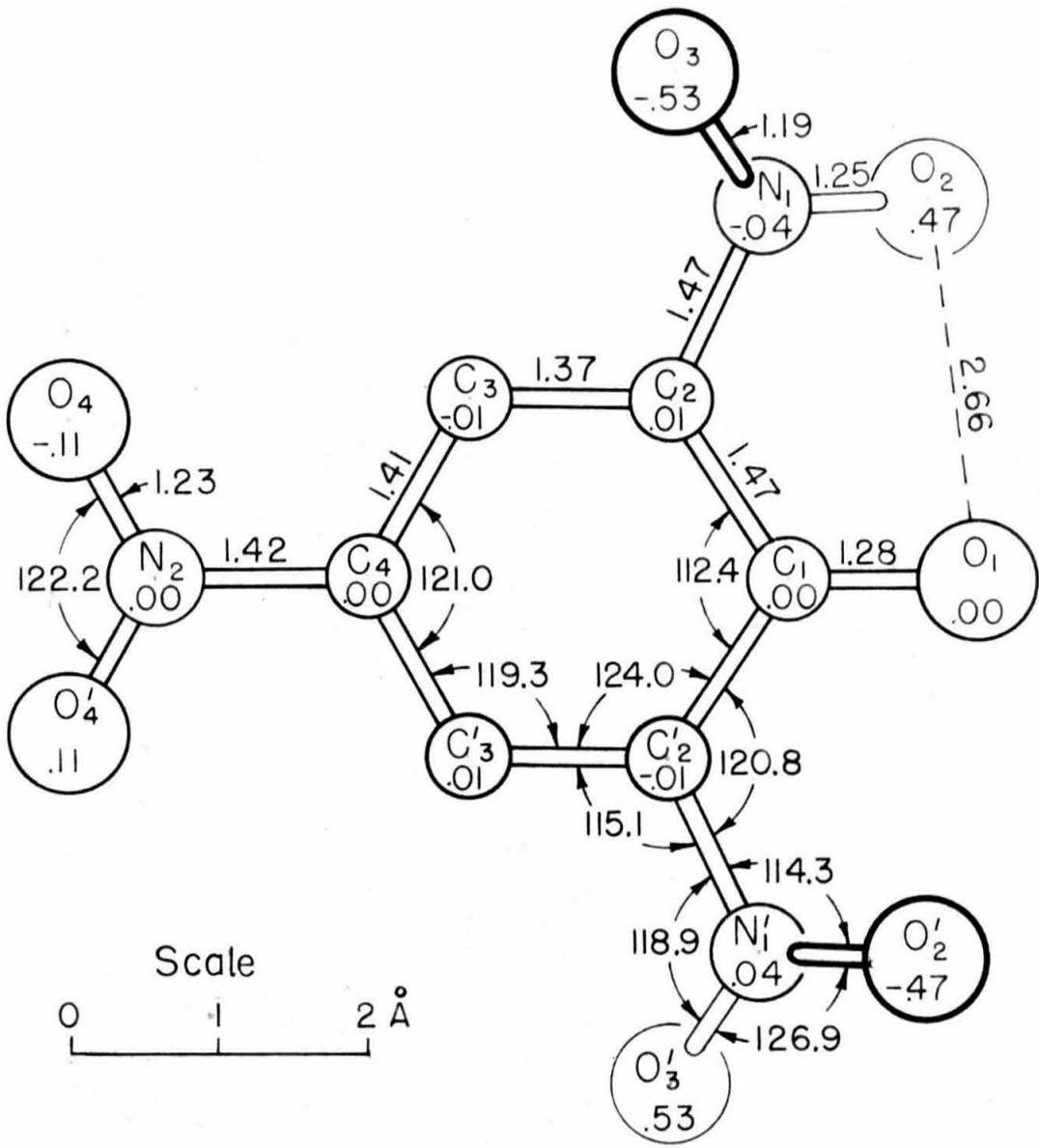


Figure 6

of the molecule are similarly related to those in the upper half by two-fold symmetry. For this reason, the bond angles have been labeled in the lower half of Figure 6, and the bond distances in the upper half.

Table IV lists all intramolecular bond lengths, the van der Waals distance between  $O_1$  and  $O_2$ , the bond angles, and the dihedral angles, all with their respective probable errors. The probable errors are calculated from the ones listed for the parameters in Table II, page 48. All lengths are in  $\overset{\circ}{\text{A}}\text{ngstroms}$  and all angles in degrees. The angle  $\alpha$  is the angle between the average plane through the benzene ring and the crystallographic plane (001), the angle  $\beta$  the dihedral angle between the benzene ring and the ortho nitro group  $O_2N_1O_3$ , and the angle  $\gamma$  is the dihedral angle between the ring and the para nitro group  $O_4N_2O_4'$ .

The  $1.28 \overset{\circ}{\text{A}} \text{C}_1\text{-O}_1$  bond is rather short, corresponding to about 50% double bond character according to the formula given by Pauling<sup>(17)</sup>. It is found, however, that all of the most stable non-Kekule type resonance structures which can be drawn, i.e. structures having a constant, maximum number of covalent bonds without free electrons or formal charges on any of the carbon atoms, involve the assignment of a double bond to  $\text{C}_1\text{-O}_1$ . The implication that resonance structures of the non-Kekule type make at least a 50% contribution to the actual structure may seem somewhat surprising. It must be kept in mind, however, that in those aromatic compounds in which the Kekule resonance forms make overwhelming contributions,

Table IV

Bond Distances and Angles with their Probable Errors

<u>Distances</u>		<u>Angles</u>	
C <sub>1</sub> -O <sub>1</sub>	1.28 ± 0.01 Å	O <sub>1</sub> C <sub>1</sub> O <sub>1</sub> '	112.4 ± 1.0°
C <sub>2</sub> -C <sub>1</sub>	1.47 ± 0.01	C <sub>1</sub> C <sub>2</sub> C <sub>3</sub>	124.0 ± 0.7
C <sub>2</sub> -N <sub>1</sub>	1.47 ± 0.01	C <sub>1</sub> C <sub>2</sub> N <sub>1</sub>	120.8 ± 0.7
C <sub>2</sub> -C <sub>3</sub>	1.37 ± 0.01	C <sub>3</sub> C <sub>2</sub> N <sub>1</sub>	115.1 ± 0.6
N <sub>1</sub> -O <sub>2</sub>	1.25 ± 0.01	C <sub>2</sub> N <sub>1</sub> O <sub>2</sub>	114.3 ± 0.7
N <sub>1</sub> -O <sub>3</sub>	1.19 ± 0.01	C <sub>2</sub> N <sub>1</sub> O <sub>3</sub>	118.9 ± 0.7
C <sub>3</sub> -C <sub>4</sub>	1.41 ± 0.01	O <sub>2</sub> N <sub>1</sub> O <sub>3</sub>	126.9 ± 0.7
C <sub>4</sub> -N <sub>2</sub>	1.42 ± 0.015	C <sub>2</sub> C <sub>3</sub> C <sub>4</sub>	119.3 ± 0.6
N <sub>2</sub> -O <sub>4</sub>	1.23 ± 0.008	C <sub>3</sub> C <sub>4</sub> C <sub>3</sub> '	121.0 ± 1.0
O <sub>1</sub> ..O <sub>2</sub>	2.66 ± 0.005	O <sub>4</sub> N <sub>2</sub> O <sub>4</sub> '	122.2 ± 1.0
		α (*)	22.4 ± 0.4
		β (*)	27.4
		γ (*)	6.1 ± 0.5

(\*) The angle α is the angle between the average plane through the benzene ring and the crystallographic plane (001), the angle β the dihedral angle between the benzene ring and the ortho nitro group O<sub>2</sub>N<sub>1</sub>O<sub>3</sub>, and the angle γ is the dihedral angle between the ring and the para nitro group O<sub>4</sub>N<sub>2</sub>O<sub>4</sub>'.

all alternate forms are not of the most stable type as defined above.

If we were to draw all of the most stable resonance forms of the picrate ion, including the Kekule types, and count the number of times each carbon-carbon bond is assigned a double bond, we would find that  $C_2-C_3$  has the most double bond character followed by  $C_3-C_4$ , while  $C_1-C_2$  has the least amount. The expected degree of double bond character therefore agrees qualitatively with the relative shortness of the observed bond lengths. The remaining three carbon-carbon bonds are, of course, related by symmetry to the ones already mentioned. The relatively low value of  $112^\circ$  for the angle  $C_2C_1C_2^1$  is in accord with the large amount of double bond character of the  $C_1-O_1$  bond and the relatively small amount of double bond character of the  $C_1-C_2$  bond. For a carbon atom forming one pure double bond and two pure single bonds one expects an angle of about  $110^\circ$  between the single bonds. For this same reason, the increase of angle  $C_1C_2C_3$  from the normal  $120^\circ$  to  $124^\circ$  is also reasonable.

The para nitro group  $O_4N_2O_4^1$  makes a dihedral angle of  $6^\circ$  with the benzene ring, the line of intersection between the two planes being the  $N_2C_4$  bond as required by symmetry. The direction of this rotation is such as to give the para nitro group a greater tilt with respect to (001) than the tilt of the benzene ring. The result of this twist is that each of the two oxygen atoms moves a little closer to a neighboring potassium ion. The twist is therefore caused by

an interionic attraction, and is not likely to exist in a free molecule. It is sufficiently small so that it is not likely to interfere much with the partial double bond character of the  $C_4N_2$  bond.

The ortho nitro group  $O_2N_1O_3$  makes a dihedral angle of  $27^\circ$  with the plane of the benzene ring. The line of intersection between the two planes is nearly colinear with the  $N_1C_2$  bond. In addition to this twist around the  $N_1C_2$  bond, the nitro group is further deformed by a rotation in its own plane about an axis perpendicular to its plane through the atom  $N_1$ , so that the angles  $C_2N_1O_2$  and  $C_2N_1O_3$  become unequal. The deformation of the ortho nitro group is caused by steric hindrance between  $O_1$  and  $O_2$ , which would be much too close to each other if the nitro group were coplanar with the benzene. Even as it is, the van der Waals distance between  $O_1$  and  $O_2$  is only  $2.66 \text{ \AA}$ , as against a normal distance of about  $2.8 \text{ \AA}$  between oxygen atoms of different molecules. This shortening is not alarming, however, since the intramolecular forces tending to squeeze the two oxygen atoms together can be of a larger order of magnitude than the London dispersion forces which are the only source of attraction in an intermolecular contact. In addition to the deformation of the N-O bonds, the steric hindrance also causes a bending back of the  $C_2N_1$  bond with the resulting small value of  $115^\circ$  for the angle  $C_3C_2N_1$ . One might even expect the  $C_2N_1$  bond to be bent appreciably out of the plane of the benzene ring but this happens not to be the case. The atom  $N_1$  is only  $0.04 \text{ \AA}$

out of the plane of the benzene ring, with a corresponding angle of less than  $2^\circ$  between the  $C_2N_1$  bond and this plane. The  $C_2N_1$  bond is seen to be longer than the  $C_4N_2$  bond. This is to be expected. The large twist of the ortho nitro group out of the benzene plane makes resonance forms with a C-N double bond less favorable than the corresponding resonance form involving the para nitro group, which is more nearly coplanar with the ring. The  $N_1O_3$  distance is shorter than  $N_1O_2$ , from which fact it is inferred that the  $N_1O_3$  bond has more double bond character with the result that atom  $O_2$  has more negative charge than atom  $O_3$ . This result is very reasonable, because the packing of the structure, described below, is such that atom  $O_2$  has two near potassium ion neighbors, whereas atom  $O_3$  has none.

#### The Packing of Potassium Picrate

Figure 7a is a projection of one complete unit cell onto (001). The thickness of the circles representing the atoms and the placement of the sticks representing chemical bonds are again adjusted so as to give an impression of depth. The numbers within or near the circles, showing the depths or z-parameters of the atoms, however, are given in units of cell edge fractions rather than in  $\text{\AA}$  as before. Figure 7d is a space group diagram which should help in clarifying the symmetry relationships between the different molecules in Figure 7a. All picrate ions lie on two-fold axes parallel to  $b_0$ , either at  $z = \frac{1}{4}c_0$  or  $z = \frac{3}{4}c_0$ . Nevertheless, the



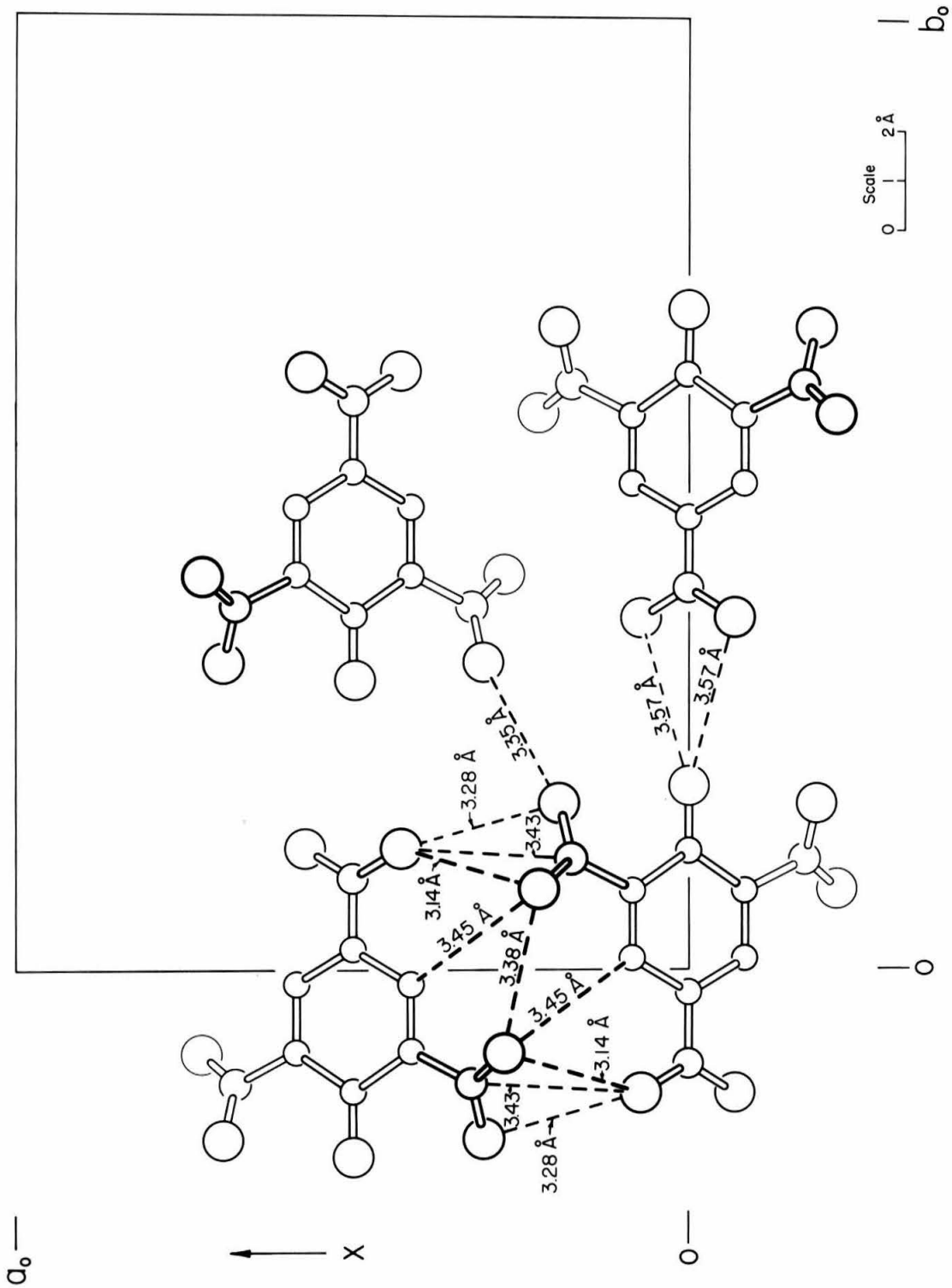


Figure 7b

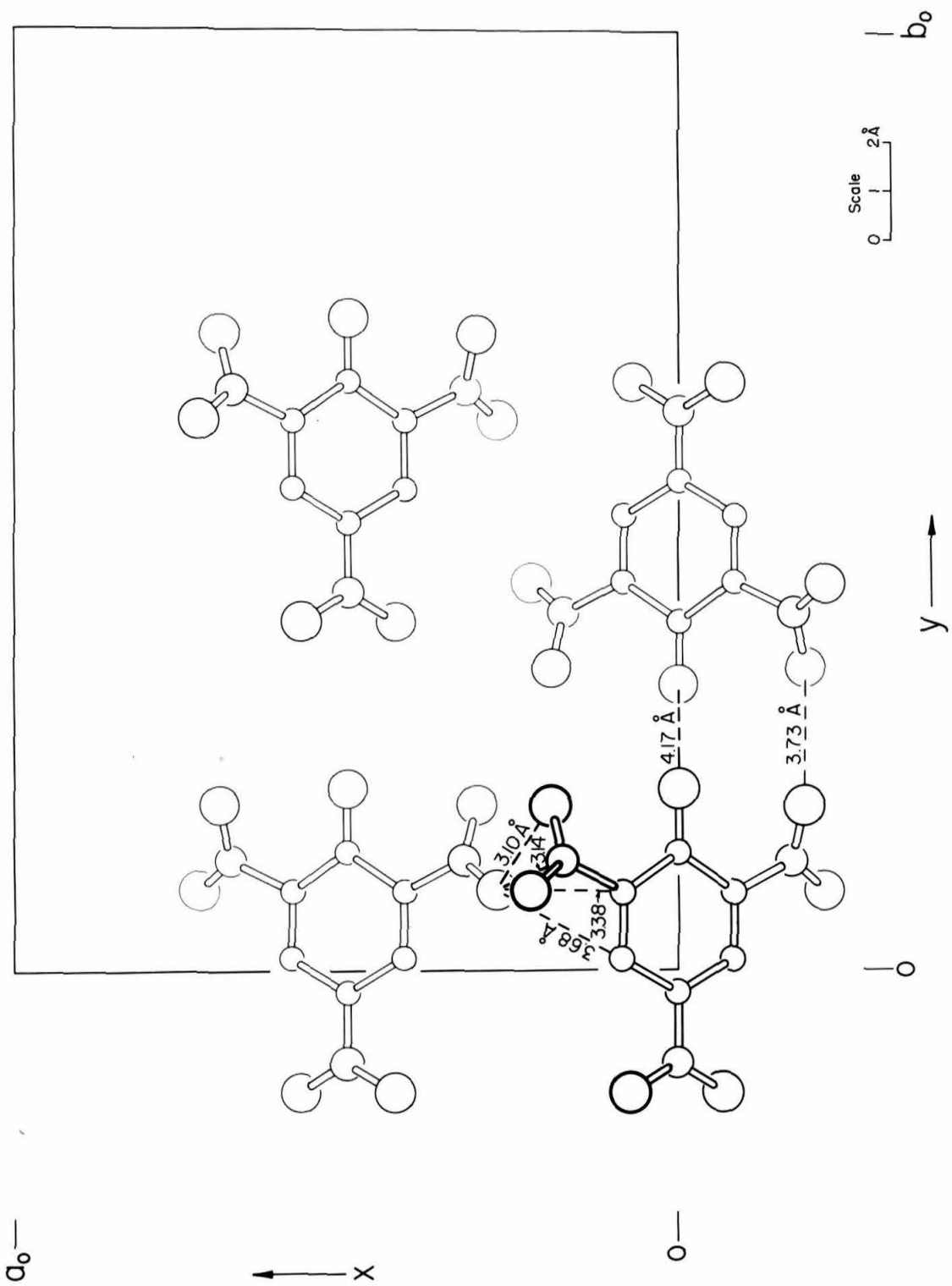


Figure 7c

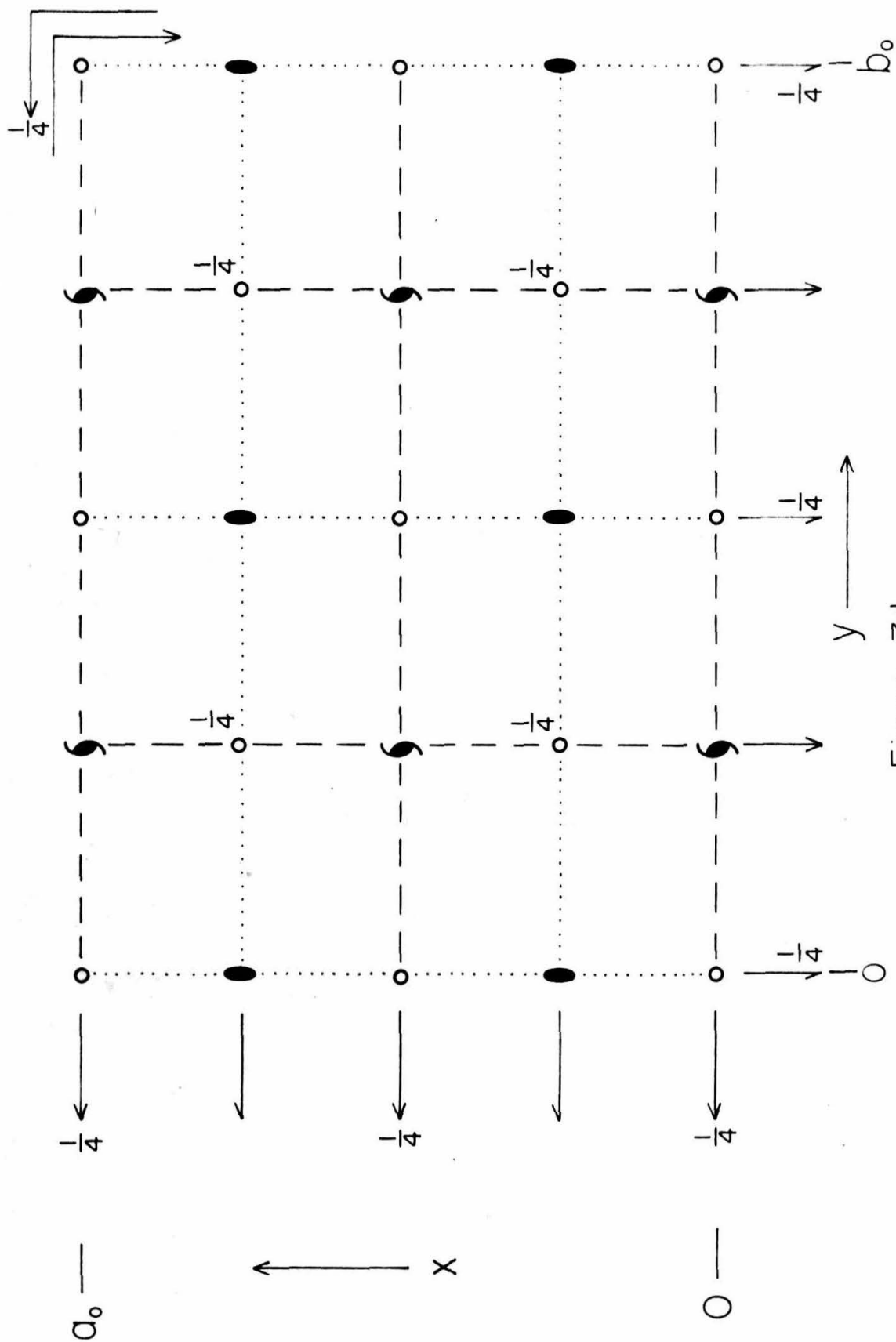


Figure 7d  
Space Group Diagram for  $D_{27h}^{27}-Ibca$

structure is not very layer-like for the following reasons. Each molecule is tipped by  $22^\circ$  relative to (001), and the ortho nitro groups are further twisted by  $27^\circ$  relative to the plane of the molecule. A molecule lying on a two-fold axis at  $z = 1/4 c_0$  therefore has atoms with z-parameters ranging from  $z = -0.002 c_0$  to  $z = 0.502 c_0$ . Furthermore, adjacent molecules in either the x or the y directions are tipped in opposite directions relative to (001). Thus, while we can formally classify all picrate molecules in the unit cell as belonging either to the "layer" at  $z = 1/4$  or to the one at  $z = 3/4$ , the structure is actually not sufficiently layerlike to provide good cleavage parallel to (001).

Adjacent picrate molecules in the z direction show a considerable amount of overlap in projection, Figure 7a. There are some rather short van der Waals contacts between them. If we consider all of the picrate ions in the structure which are more or less directly underneath each other in the z direction, they form what will hereafter be referred to as a "stack". All the molecules in a stack have parallel benzene rings, all being tipped in the same direction relative to (001). Adjacent molecules in a stack are related by a center of symmetry between them and are therefore relatively enantiomorphous. Molecules in a neighboring stack are all tilted by the same amount,  $22^\circ$ , but in the opposite direction relative to (001). The intermolecular distances within a stack will be described in detail later.

Figure 7b is a projection of all the picrate ions in one

"layer", e.g. all the ions whose two-fold axes lie at  $z = \frac{1}{4} c_0$ . The potassium ions are omitted from this drawing entirely. The shortest intermolecular distances are indicated by dotted lines, and the value of these distances in Angstroms\* is indicated by numbers in the diagram. For further reference the following values will be accepted as normal van der Waals radii<sup>(18)</sup>: N = 1.5 Å, O = 1.4 Å; the half thickness of an aromatic molecule is given as 1.85 Å and this will be taken as the van der Waals radius for carbon even when the direction of the link is not quite perpendicular to the plane of the ring. We can now draw some conclusions regarding the existence of van der Waals bonds by comparing the intermolecular distances in the various diagrams with the appropriate combinations of radii from the preceding list. Figure 7b shows that there are no good van der Waals contacts between picrate ions situated on the same two-fold axes. There are a few contacts between a given picrate ion and a neighboring one in the same layer in the x direction. All these distances, however, are at least somewhat longer than the optimum values obtained from the corresponding radius sum. Figure 7c is again a projection onto (001), showing one molecule centered at  $z = \frac{1}{4}$  and all the molecules in the layer above except the one in the same "stack". Both figures 7b and 7c are, of course, excerpts from Figure 7a. The shortest intermolecular

---

\* The units used in Figures 7a, 7b, and 7c are hybrid for the sake of convenience. The van der Waals distances are given in Angstroms, while the z-parameters are given in fractions of the  $c_0$  axis so that atoms in special positions are recognizable by their z-parameters, such as 0,  $\frac{1}{4}$ ,  $\frac{1}{2}$ , or  $\frac{3}{4}$ .

distances are again shown by dotted lines, with the values of the distances written beside them. Here again there are no contacts of importance in the y direction. In the x direction there are a few short contacts between picrate ions related by the c-glide plane at  $x = 1/4$ , but even these contacts are in all cases at least somewhat longer, by about  $0.2 \text{ \AA}$ , than the normal radius sums.

The question then comes up as to what is holding the structure together. In the  $c_0$  direction we have the van der Waals cohesion within the stacks, as already mentioned, plus ionic binding, as we shall see below. Let us refer back to Figure 7a and consider the potassium ion at  $(0.133, \frac{1}{4}, \frac{1}{2})$  in cell edge fractions. Like all the other potassium ions it is surrounded by eight oxygens from various picrate ions, all of them having a partial negative charge. There are two oxygens each at distances of 2.73, 2.78, 2.84, and  $2.97 \text{ \AA}$ .  $2.73 \text{ \AA}$  is about normal for a potassium-oxygen ionic distance, and the other distances are within reasonable range of this, considering the fact that ionic forces and even ion - dipole forces do not fall off as rapidly as chemical or van der Waals bindings. The atoms of type  $O_1$  are at the shortest distances of  $2.73 \text{ \AA}$ . Atom  $O_1$  can be expected to have about half an electronic charge if we assume that the Kekule structures contribute about 50% to the actual structure of the picrate ion. Atom  $O_1$  incidentally is shared by two equidistant potassium ions, the one in question plus

another one at  $(-.133, \frac{1}{4}, 0)$ . Atom O<sub>4</sub> is at the next shortest distance of 2.78 Å, and is not shared with any other potassium ion. It can be expected to have more than half an electronic charge. It obtains half a negative charge from local nitro group resonance, plus material amount of extra charge from the non-Kekule structure in which both the O<sub>4</sub> and O<sub>4</sub>' atoms are assigned formal negative charges. In all of the most stable resonance structures, therefore, atom O<sub>4</sub> is assigned either a half or a full negative charge. On the other hand, the effectiveness of this rather large negative charge is reduced by the vicinity of the positively charged N<sub>2</sub> atom, so that the interaction between atom O<sub>4</sub> and the potassium ion is of the less energetic ion - dipole type. Roughly the same situation holds for the two O<sub>2</sub> atoms at distances of 2.84 Å from the potassium. Due to the twist of the ortho nitro group relative to the benzene ring, the non-Kekule structure in which atom O<sub>2</sub> is assigned a full negative charge makes a smaller contribution than the similar resonance form involving a full negative charge on atom O<sub>4</sub>. On the other hand, in all the other resonance forms atom O<sub>2</sub> is assigned a little more than half of a negative charge at the expense of atom O<sub>3</sub>, which prefers more double bond character. This is probably because atom O<sub>3</sub> is not in the vicinity of any potassium ions. The particular potassium ion we have been discussing has two more O<sub>2</sub> neighbors at the longer distance of 2.97 Å. These, however, are simultaneously shared by other potassium ions to which they are bound by the shorter, normal K...O<sub>2</sub> distance

of 2.84 Å. One fact which is easily discernible from the projection onto (001), Figure 7a, is that the potassium ions provide very good ionic binding for the structure in the  $y$  direction, across the planes  $y = \frac{1}{4}$ . Half of the surrounding oxygen atoms belong to picrate ions to the left of this plane, in the negative  $y$  direction, the other half belong to molecules in the positive  $y$  direction from the potassium. Furthermore, the  $K^+$  ion provides good binding in the  $z$  direction, across the plane  $z = \frac{1}{2}$ , since half of the surrounding oxygen atoms belong to picrate ions centered around  $z = \frac{1}{4}$ , while the other half belong to picrate ions whose centers are at  $z = \frac{3}{4}$ .

Figure 8 is a projection of two potassium ions with their surrounding oxygen atoms onto the plane  $y = \frac{1}{4}$ , which is parallel to (010). The numbers in the circles representing atoms refer to the depth in Angstroms of these atoms relative to the plane of the paper. The coordination polyhedron of oxygens around each potassium has the shape of a distorted square Archimedean antiprism. The trace of the plane  $x = \frac{1}{4}$ , perpendicular to the plane of the paper, is indicated by a dashed line. Across this plane the only ionic binding in the structure is that derived from the sharing of  $O_2$  type atoms between neighboring potassiums. This binding is relatively weak, particularly because each  $O_2$  atom so shared is connected by a normal distance to only one of the potassiums, and by a longer distance to the other. The weak ionic binding across the plane  $x = \frac{1}{4}$  is augmented somewhat by a few van der Waals contacts between picrate ions across this plane, discussed previously in

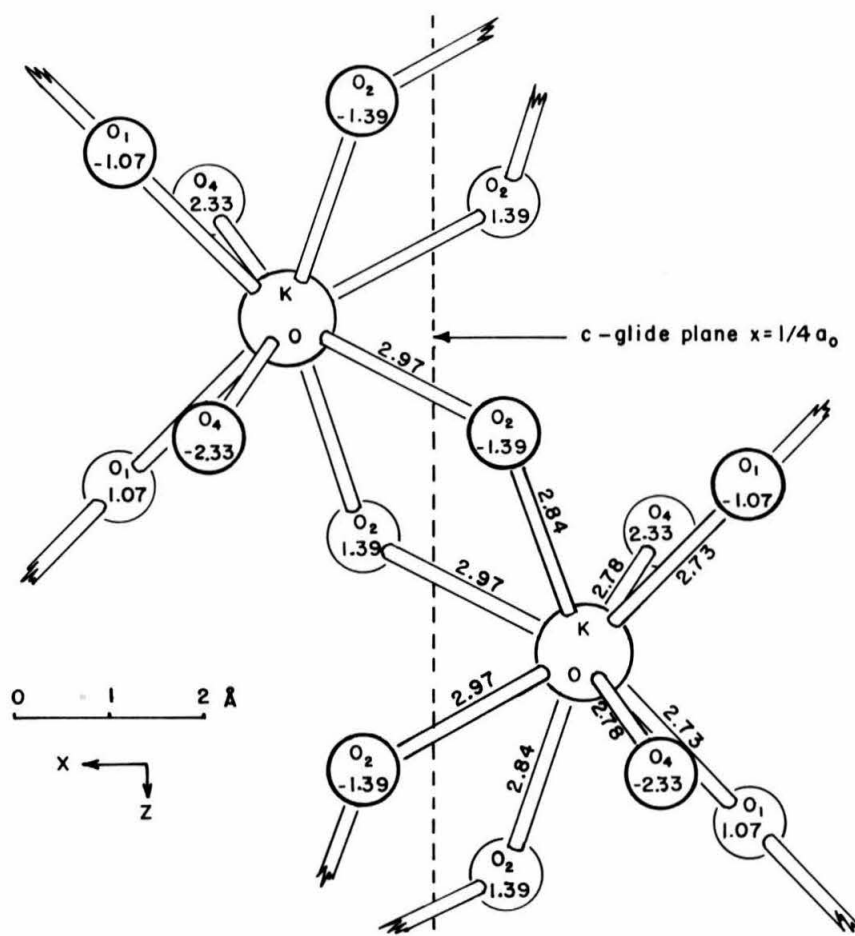


Figure 8

connection with Figures 7a and 7b. It is therefore not surprising that the principal cleavage in potassium picrate, as reported in Groth<sup>(9)</sup>, occurs parallel to (100). Atoms of type  $O_1$  are also shared with neighboring potassium ions, not shown in Figure 8. This kind of sharing is not important for the cohesion of the structure along the x direction, as a reference back to Figure 7a will show quite clearly. However, it has the result that all potassium ions in the structure which lie in the plane  $y = \frac{1}{4}$  are mutually interconnected by the sharing of coordination polyhedra. The same is true, of course, for all the potassium ions in the plane  $y = \frac{3}{4}$ , and for all the other planes related to these two by lattice translations. The binding which the potassium ions provide in the z direction is augmented by the van der Waals contacts between adjacent picrate ions in a stack, which will now be discussed.

Figures 9a and 9b are schematic representations of a portion of a stack, the molecules being represented by slabs. Figure 9a is a perspective view while 9b is the corresponding projected side view. Each slab is tilted  $22^\circ$  relative to the  $c_0$  axis, but the latter passes through equivalent points in all of them, so that the stack as a whole is parallel to  $c_0$ . Figure 10 shows two adjacent picrate ions in a stack, projected onto (100). The numbers in the circles are the x-parameters, in  $\overset{\circ}{\text{A}}$ , of the atoms. The two molecules are mirror images of each other as previously mentioned. The dashed lines represent van der Waals contacts whose lengths are also

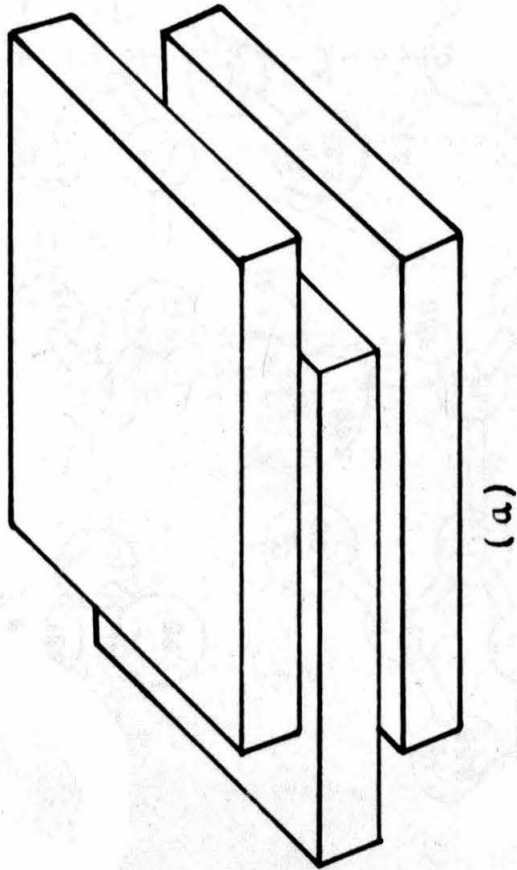
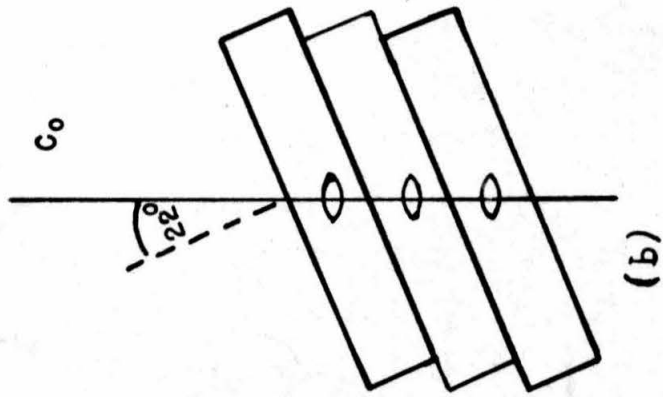


Figure 9

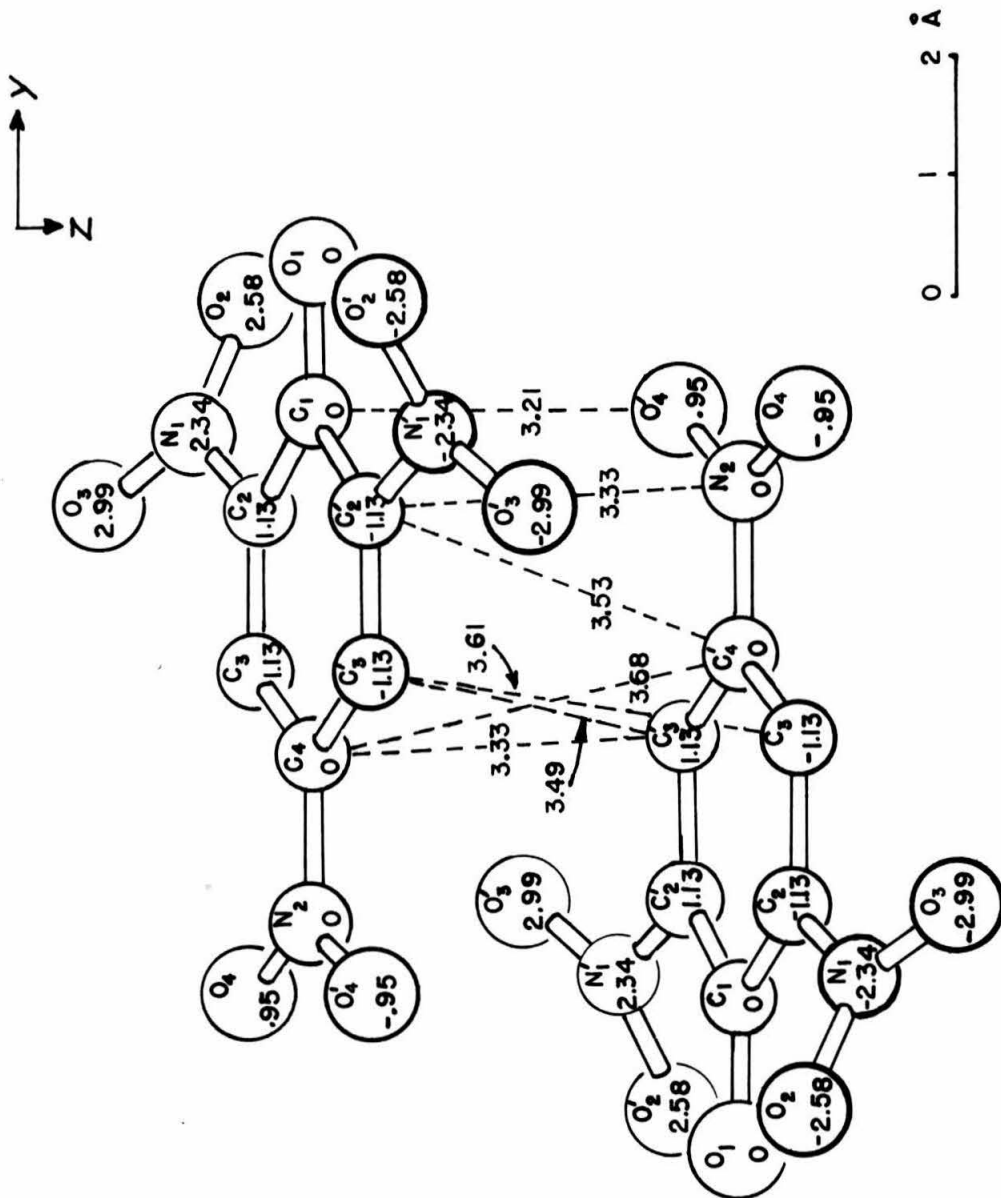


Figure 10

given in the drawing. According to our list of van der Waals radii, the distances  $C_1..O_4'$ ,  $C_2'..N_2$ ,  $C_3'..C_3$ , and  $C_4..C_4$  are about normal\*,  $C_2'..C_4$  and  $C_3'..C_3'$  are somewhat shorter, and  $C_4..C_3'$  is definitely on the short side, being about 0.4 Å shorter than the expected 3.7 Å. It is not unique, however. In graphite, for instance, the interatomic distance between layers is about 3.4 Å. All other intermolecular distances between the two picrate ions are longer than the sum of the van der Waals radii concerned and therefore of no particular interest.

The shortness of some of these intermolecular distances may be due to larger than normal London dispersion forces, caused by some kind of synchronized oscillation of charges over the whole extent of these highly conjugated molecules. There have been some speculations of this type in the literature. See for instance a recent paper by S. Freed and K. M. Sancier<sup>(19)</sup> and their reference to an earlier paper by F. London. On the other hand, the whole packing of the structure may be determined solely by the packing of oxygens around the potassium ions, and the short intermolecular distances between picrate molecules may be merely a matter of compression. It is probable that there is no permanent dipole -- permanent dipole attraction between two adjacent picrate ions in a stack. In the first place, each molecule

\* The following notation is used for these van der Waals distances: In  $A_i..B_j$ ,  $A_i$  is an atom from the upper molecule in the diagram,  $B_j$  from the lower molecule in Figure 10.

has a net negative charge distributed over its whole periphery. In the second place, the shortest approaches occur between symmetrically equivalent portions of two molecules, i.e. between the  $C_3C_4C_3'$  region of one and the corresponding region of the other.

#### Comparison with Similar Structures

Some of the results of the determination of similar compounds, referred to in the introduction, will now be given. The determination of the most similar of these compounds is perhaps the determination of picryl iodide by Powell<sup>(4)</sup>. The ortho nitro groups in picryl iodide are twisted out of the plane of the benzene ring by about  $80^\circ$ , due to the large iodine atom. The ortho C-N bonds have a length of  $1.45 \text{ \AA}$ , the para C-N bond a length of  $1.35 \text{ \AA}$ . The benzene ring is reported to be a regular hexagon with edges equal to  $1.39 \text{ \AA}$ . The ONO angles of the ortho and the para nitro groups are, respectively,  $127^\circ$  and  $120^\circ$ . Powell reports one intermolecular O...C distance as short as  $3.1 \text{ \AA}$ . All other intermolecular distances are longer than the corresponding van der Waals radius sum. Individual distances in this determination are quite unreliable. The structure was determined by Fourier projections which are dominated by the iodine peaks. The rest of the molecule shows up just enough to deduce its overall position and orientation. The actual bond lengths quoted are probably based to a large extent on a priori assumptions.

The structure of meta-dinitrobenzene has been investigated by Gregory and Lassetre<sup>(7)</sup> and also by Archer<sup>(6)</sup>.

The results in each case are based on projections and on some assumptions. The two determinations show considerable differences in bond lengths and angles but agree on the crude features of the structure. Neither of them is reliable with regard to details. They do agree, however, on the very short intermolecular distance of  $2.95 \text{ \AA}$  between a nitro oxygen and a CH group of another molecule.

Paradinitrobenzene has been investigated three times. The first investigation by James, King, and Horrocks<sup>(1)</sup> will not be elaborated on here because it has been superseded by the two later investigations. Llewellyn<sup>(2)</sup> determined the structure of this compound by three dimensional Fourier methods without, however, correcting for the finite series errors. He estimates the error limits of his bond lengths as  $0.02 \text{ \AA}$ , a value which is undoubtedly much too optimistic. The errors due to the termination in the Fourier series alone can amount to about  $0.06 \text{ \AA}$  for the parameters and consequently about  $0.08 \text{ \AA}$  for the bond lengths. His discrepancy, or reliability factor, is 24%, which is rather high. He reports the following results: All C-C bonds are  $1.385 \text{ \AA}$  in length. All C-N =  $1.41 \text{ \AA}$ , and all N-O =  $1.23 \text{ \AA}$ . The angles ONO are  $124^\circ$ . The whole molecule is described as symmetrical and planar. Actually, Llewellyn's statement that the nitro groups are coplanar with the benzene ring is incompatible with his own parameters, which lead to an angle of tip of  $11.7^\circ$  of the nitro groups relative to the benzene ring. Abrahams<sup>(3)</sup> published a subsequent paper on paradinitrobenzene, in which

he also discussed possible sources of error that might have affected Llewellyn's work. Abrahams' determination was based on Fourier projections only. He reports a C-N length of 1.48 Å. Otherwise his results are fairly similar to those of Llewellyn. Abrahams expresses the opinion that neither of the two determinations is very trustworthy in detail.

The structure of paranitroaniline has been investigated by Abrahams and Robertson<sup>(8)</sup> by means of two dimensional Fourier projection methods. The authors report C-C bond lengths varying from 1.31 to 1.39 Å, but do not ascribe any significance to these variations because of the rather large uncertainty of some of the parameter values. The variations are such as to completely contradict the predictions of resonance theory. The N-O distances are reported as 1.26 Å. The carbon to nitro-group-nitrogen distance is given as 1.39 Å. The carbon to amine-nitrogen distance is reported to be 1.36 Å. The authors report a phenomenally short intermolecular distance of 2.7 Å between a nitro group oxygen atom and the CH group ortho to the amine group of another molecule. The authors speculate that there is a new type of interaction involved here, the same interaction that causes the formation of molecular compounds between aromatic molecules of this type. They feel that paranitro aniline is forming a self complex in its crystal structure.

The last compound which will be discussed here is N-picryl-paraiodoaniline. Grison<sup>(5)</sup> reported the structures of three polymorphic variations of this compound, based on Fourier projections and some three dimensional Fourier

sections. The molecules in the three variations are very similar and merely pack differently. The presence of the heavily scattering iodine atom made accurate bond length determinations difficult, but Grison lists the average length of each bond species and estimates these averages to be correct to about 0.05 Å. Their values are as follows: C-C = 1.40 Å, C-N = 1.40 Å, N-O = 1.23 Å, C-NH = 1.45 Å, and C-I = 2.1 Å. The oxygen-oxygen distance within a nitro group is 2.20 Å with a consequent ONO angle of 127°. One of the ortho nitro groups makes an angle of 28° with the benzene ring to which it is attached. The O..H-N distance is 2.75 Å and presumably contains a hydrogen bond. The other ortho nitro group is twisted out of the plane of the picryl benzene ring by 55°. This large twist is due to an additional steric hindrance between the ortho nitro group and the second benzene ring. The steric hindrance affecting both ortho nitro groups is thus affected by factors which are not present in the case of potassium picrate.

REFERENCES

1. R. W. James, G. King, and H. Horrocks, Proc. Roy. Soc., A 153, 225, (1935).
2. F. J. Llewellyn, J. Chem. Soc., 1947, p. 884.
3. S. C. Abrahams, Acta. Cryst., 3, 194, (1950).
4. M. Powell, J. Chem. Soc., 1940, p. 1398 - 1402.
5. Emmanuel Grison, Acta. Cryst., 2, 410, (1949).
6. E. M. Archer, Proc. Roy. Soc., A 188, 51-62, (1946).
7. N. W. Gregory and E. N. Lasettre, J. Am. Chem. Soc., 69, 102, (1947).
8. S. C. Abrahams and J. M. Robertson, Acta. Cryst., 1, 252-59, (1948).
9. P. Groth, "Chemische Kristallographie", Wilhelm Engelmann, Leipzig, 1917, vol. IV, p. 117-8.
10. M. J. Buerger, "X-Ray Crystallography", John Wiley & Sons, New York, p. 252.
11. De Lang, Robertson, and Woodward, Proc. Roy. Soc., A 171, 398, (1939).
12. Whittaker and Robinson "The Calculus of Observations", 2nd Ed., Blackie & Sons, London, 1937.
13. "Internationale Tabellen zur Bestimmung von Kristallstrukturen", vol. 1, Gebrueder Borntraeger, Berlin, 1935. p. 149-50.
14. C. A. Beevers and H. Lipson, Phil. Mag., 17, 855 (1934).
15. E. W. Hughes, J. Am. Chem. Soc., 63, 1737, (1941).
16. Reference (10), p. 227.
17. Linus Pauling "The Nature of the Chemical Bond", Cornell University Press, Ithaca, N.Y., 2nd Ed., p. 175, formula 22-2.
18. Reference (17), page 189.
19. Simon Freed and Kenneth M. Soncier, J. Am. Chem. Soc., 74, 1273, (1952).

## PROPOSITIONS

1. It is frequently very difficult to determine the density of small crystals of alloys. The flotation method usually cannot be used because it is not possible to find liquids of sufficiently high densities. I propose that the density of individual crystals can be determined by a dynamic method. It should be possible to calculate the density of a crystal by measuring its rate of fall in several liquids of known and different densities and viscosities.

2. The systematic study of all polyhedra up to a certain degree of complexity (e.g. 20 vertices) would be of interest with respect to the determination and description of metal structures. Such a study was started once at this Institute by Mr. Robert P. Smith<sup>(1)</sup>. The equation  $V + F = E + 2$ , due to Euler, was useful in this work. This equation relates the number of vertices  $V$  and the number of faces  $F$  to the number of edges  $E$  in the general class of polyhedra which can be deformed into a sphere. Mr. Smith found, however, that there are combinations of  $V$ ,  $F$ , and  $E$  which satisfy the Euler relation but do not correspond to any possible polyhedra.

I propose that there are at least two more necessary conditions for the existence of polyhedra with a given combination of  $E$ ,  $V$ , and  $F$ . These conditions are the two inequalities  $F + 4 \leq 2V \leq 4F - 8$ .

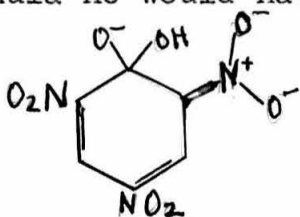
3. The most conveniently built models of complex metal or mineral structures are of the ball and rod type. All the balls are situated on vertical rods which are stuck in a single base plate. However, the density of rods often confuses the viewer and obscures structural details. It should be possible to make these rods out of a transparent material and to immerse the model in a liquid of the same refractive index as that of the transparent rods. The rods need not have much mechanical strength because of the buoyancy of the liquid.

4. In the determination of the structure of potassium picrate I have noticed that if the temperature factors are determined separately for the various layerlines, the values of the temperature factor parameters increase with increasing layer line number. Mr. Harry Yakel<sup>(2)</sup> noticed the same effect in the determination of the structure of NN'-diglycyl-L-cystine. I propose that this effect may be general enough to be worth investigating. I can offer a possible qualitative explanation which would have to be checked by numerical calculations.

5. Some old papers have been found which deal with the color produced by heat and alkali treatment in picric acid, picrates, and similar polynitro aromatic compounds. There seem to have been two schools of thought. One, exemplified by

Dehn and Ball<sup>(3)</sup>, believed in a tautomeric equilibrium between a colored and an uncolored form of the acid. The uncolored form was believed to be of the "benzoid" type with a formula as it is now usually written. The colored form was supposed to be of the "quinoid" type, with the acid hydrogen shifted to one of the nitro groups. In aqueous solution an intermediate type was believed possible, consisting of a picric acid molecule with a water molecule added to one of the nitro groups.

The other school of thought, exemplified by Meissenheimer<sup>(4)</sup>, believed that the color was due to a molecule formed from the polynitro aromatic molecule by the addition of an alkali ion, either alkoxide or hydroxide. Meissenheimer did not deal with the particular case picric acid, but by analogy the formula he would have drawn is shown here.

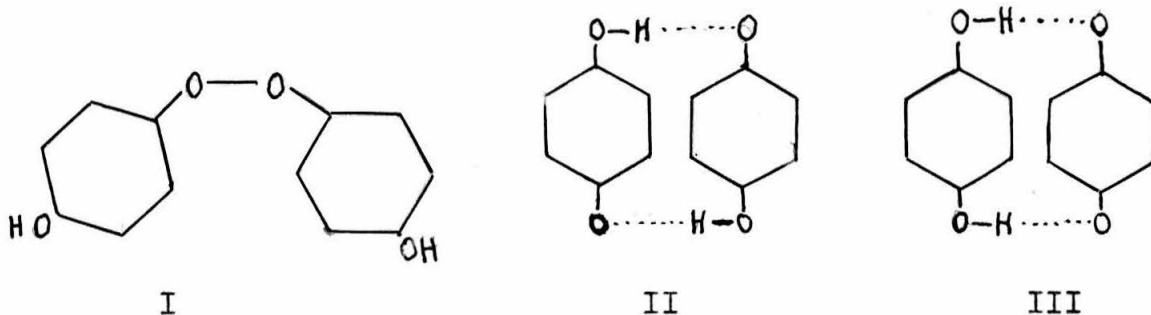


(three resonance forms)

Both schools of thought maintain that the reaction is reversible by the addition of acid, and some heating if necessary.

From some observations I have made I propose that the theory of Meissenheimer may be correct as a first step, but that sufficiently harsh treatment by heat and alkali produces a dark brown impurity which is the product of some drastic and irreversible chemical change.

6. Wheland<sup>(5)</sup> discusses the possible structure of the dimer of semiquinone, which can alternatively be considered an addition complex between quinone and hydroquinone. Michaelis and coworkers<sup>(6)</sup> have found this addition compound to be one of many components of the complex equilibrium mixture of a quinhydrone in water or alcohol. Wheland discusses I, II, and III as possible structures.



Structure II or III was proposed by Michaelis. The benzene rings in these two structures must be considered face to face. Wheland rejects I on the basis that it is not likely to be intensely colored. He likes either II or III, stating that it is not possible to make a choice between them.

I propose:

(a) Between II and III, II is much likelier to account for the color.

(b) Neither II nor III is very likely on the basis of stereochemical considerations. Furthermore, benzoquinone and the dimethyl ether of its hydroquinone seem to be able to form a quinhydrone without the benefit of hydrogen bonding.

(c) There are other possible structures besides the ones discussed by Wheland.

7. The structure of paranitroaniline has been determined approximately by Abrahams and Robertson<sup>(7)</sup> by means of Fourier projections. The authors report a phenomenally short O...CH intermolecular distance of 2.7 Å. This is somewhat shorter even than the distance one would expect, by analogy, for a hypothetical oxygen to carbon hydrogen bond. I propose that this structure be carefully and accurately reinvestigated.

8. By measuring the directional preference in the absorption of polarized infrared light by partially oriented solids ("linear crystals"), R. J. Francel<sup>(8)</sup> in a recent paper drew some conclusions about the structures of several substituted nitrobenzenes. Specifically, he tested whether the nitro groups in these compounds are coplanar with the benzene ring. He concluded that the nitro groups are coplanar with the ring in o-nitrophenol, 2-nitroresorcinol, and o-nitroaniline. The author tries to correlate these results with structural theory by quoting "The Nature of the Chemical Bond"<sup>(9)</sup>. It is stated there on page 328 that the hydroxyl group and the nitro group in o-nitrophenol are coplanar with the ring and that the resulting distance between the phenol oxygen and the nearest oxygen of the nitro group is 2.6 Å, about right for a hydrogen bond.

I submit that this is a miscalculation. The correct value must be somewhat less than 2.5 Å and the nitro group needs to be twisted out of the plane of the benzene ring by about 30° to lengthen this value to 2.6 Å. The method used by Francel, though it looks good on paper, must be rather insensitive.

9. It seems somewhat surprising that water does not denature proteins by breaking up hydrogen bonds. Other hydrogen bonding agents such as urea and guanidinium salts are believed to denature proteins in this manner. Water, on the other hand, is believed to break hydrogen bonds in cellulose, evidence of which are the weakened mechanical properties of wet paper. This specificity in the hydrogen bond breaking power of micromolecules suggests that this power is not merely a function of their ability to form good hydrogen bonds. The criterion for the occurrence of this bond breaking process may be that the energy of the hydrogen bond between the micromolecules should closely match that of the hydrogen bonds within the macromolecule.

10. It is pointed out to the chemistry faculty that propositioning is probably illegal in the city of Pasadena.

REFERENCES

1. Unpublished work.
2. Harry Yakel, Thesis, California Institute of Technology, 1952.
3. W. M. Dehn and Alice A. Ball, J. Am. Chem. Soc., 39, 1381, (1917).
4. Jacob Meissenheimer, Ann., 323, 221, (1902).
5. G. W. Wheland, "Advanced Organic Chemistry", John Wiley and Sons, 2nd Ed., p. 54 ff.
6. L. Michaelis, Chem. Revs., 16, 243, (1935),  
L. Michaelis and M. P. Schubert, Chem. Revs., 22, 437, (1938)  
and many further papers by Michaelis and coworkers in J. Am. Chem. Soc.
7. S. C. Abrahams and J. M. Robertson, Acta. Cryst., 1, 252 (1948).
8. Rudolf J. Francel, J. Am. Chem. Soc., 74, 1265, (1952).
9. L. Pauling, "The Nature of the Chemical Bond", Cornell University Press, Ithaca, N. Y., 1942, p. 222.